Biophysical Journal, Volume *110*

Supplemental Information

A Mechanism for Cytoplasmic Streaming: Kinesin-Driven Alignment of Microtubules and Fast Fluid Flows

Corey E. Monteith, Matthew E. Brunner, Inna Djagaeva, Anthony M. Bielecki, Joshua M. Deutsch, and William M. Saxton

Supporting Material

A mechanism for cytoplasmic streaming: Kinesin-driven alignment of microtubules and fast fluid flows.

Corey E. Monteith, Matthew E. Brunnner, Inna Djagaeva, Anthony Bielecki, Joshua M. Deutsch, William M. Saxton

1 Movie Legends

Movie S1

Weak correlation of microtubule motion and bending during slow cytoplasmic streaming. Live stage 9 Drosophila oocytes containing GFP-α-tubulin expressed in the germline were dissected, mounted in halocarbon oil, and fluorescence was recorded at $5sec$ intervals using an inverted Ultraview spinning disk confocal microscope. The image series is played back here at 30 $frames/sec$. The optical section is $5-10\mu m$ inward from the oocyte membrane (see Fig. 1A,B).

Movie S2

Strong correlation of microtubule motion and bending behavior during fast cytoplasmic streaming. GFP-tubulin fluorescence images were recorded in Stage 10B oocytes at $5sec$ intervals and are played back at 30 $frames/second$ (see Fig. 1C,D). The optical section, $5-10\mu m$ inward from the oocyte membrane, cuts through subcortical cytoplasm in some areas, producing

views of bright, ordered parallel arrays of undulating microtubules and of fast moving yolk endosomes (dark spheres). In other areas, where the section is shallower and cuts through the cortex, yolk endosomes associated with the cortex move slowly in the directions of overlying fast flows.

Movie S3

Endosome and lipid droplet fast streaming motion. Time-lapse confocal fluorescence images of a stage 10B oocyte showing endosomes containing trypan blue dye (red fluorescence) and lipid droplets tagged with GFP-LD (green fluorescence) expressed just in the germline. Images were collected in both channels at 2 *sec* intervals, and are played back at 30 $Frames/sec$. The oocyte nucleus is seen as a dark sphere in the top left. Note the varying fast streaming flow patterns.

Movie S4

A simulation of single filament bending behavior induced by kinesin forces. The filament has microtubule-like stiffness and forces tangent to its axis at all points like those generated by kinesin-cargo complexes moving through cytoplasm toward the free plus-end (see Fig. 5 and Supporting Material 4.6). Those plus-end directed walking forces, if unopposed, would propel the filament with its minus end leading, but its minus-end (white sphere) is tethered in space. It can rotate, but not translate. A second force, representing a cytoplasmic streaming flow field is imposed on the system, moving constantly from the bottom to the top of the field of view. Repeated simulations consistently developed stable rotating helical wave forms, with handedness depending on the details of random initial filament configurations. Analytical solutions with reasonable values for microtubule stiffness, and kinesin force predict a radius of curvature of $24 - 54\mu m$, which is roughly one third the width of a stage 10B oocyte. To facilitate recognition of the bending behavior, the width of the filament here is scaled up to 2,000-fold that of a real microtubule.

Movie S5

A simulation of single filament bending behavior when adjacent to an impenetrable wall. These parameters are the same as in Movie S4 but the system differs by the addition of a barrier that is parallel to the microtubule. This changes the travelling helical wave to a shape similar to a sinusoidal wave that is very well described by the mathematical analysis of Sec. 4.4. When the cytoplasmic streaming flow field is slower, the shape becomes similar to prolate cycloids that are also well described by the same analysis.

Movie S6

A simulation of the bending behaviors of 100 filaments with minus-ends tethered near a barrier to filament and fluid motions. The axis of each filament is initially in a random configuration (see Fig. 6A and Supporting Material Sec. 5.11)) that changes due to interactions of microtubule-like stiffness, kinesin-like fluid-filament shear forces tangent to each filament at all points, and hydrodynamics as described in the Supporting Material, Sec. 5 (parameters as in Fig. S16(d)). Filament length is 16 (dimensionless units), at an elevation of $H = 1$ above a membrane-like wall. The velocity field at the wall vanishes, which suppresses hydrodynamic interactions between microtubules. In this case, the elevation of minus-ends is too low to allow for long-range filament correlation and organized fast streaming.

Movie S7

A simulation of the bending behaviors of 100 filaments with elevated minus end tether points. The parameters are as described for Movie S6, except that minus-ends are tethered above the membrane barrier at $H = 2$ (see Fig. 6B; parameters as in Fig. S16c). In this case fluid motion between the minus-ends and the wall allow strong hydrodynamic interactions between microtubules that create long-range correlated behaviors and robust fast streaming. At higher minus-end tethering elevations, correlation becomes stronger and microtubule bending behavior is diminished, generating relatively straight stable arrays.

Movie S8

FRAP evidence for cortical tethering of microtubules. High magnification GFP-tubulin images recorded with an Olympus 2-photon microscope in a stage 10B oocyte at 0.93 *sec* intervals are played back here at 30 $frames/sec$. High intensity excitation was used to photobleach a shallow $10 \times 30\mu m$ area in subcortical arrays of microtubules. Note that the photobleached area remains stationary as fluorescence recovers, while organelles that exclude GFP-tubulin stream past. Adjacent non-streaming organelles are associated with the cortex. Quantification and other details of this experiment are presented in Fig. 7.

2 Enhancement of Streaming Due to Hydrodynamics

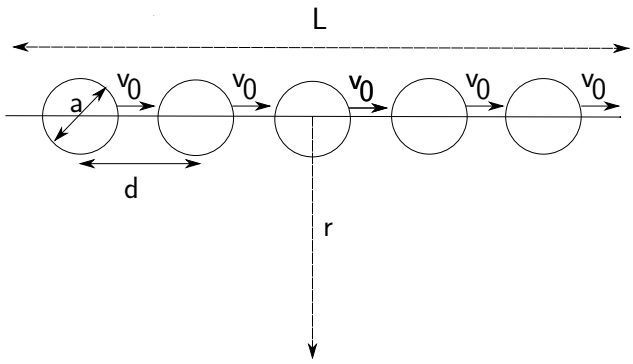

Figure S1: **Fluid movement by viscous drag on a train of impellers at low Reynolds number.** A train of spherically shaped impellers of diameter a and separation d, all moving in a fluid with a velocity v_0. The velocity $v(r)$ is measured at a point a distance r from the axis.

Consider objects that can move surrounding fluid by viscous drag, referred to as "impellers" here. Each impeller has a maximum linear dimension a, and has a mean spacing of d, arranged in a straight line as shown in Fig S1, reproduced from Fig 2 of our accompanying paper. These impellers are pictured as spheres, but hydrodynamics is not sensitive to the exact shape of an

impeller, as it depends mainly on its maximum linear dimension [18]. We will now analyze the amount of streaming due to motion of these impellers moving on a single microtubule. We initially consider the impellers to be much larger than the kinesin molecules so that they dominate the hydrodynamical response of the fluid.

If spherical impellers were close-packed along the microtubule, that is $a \approx d$, then this problem would be equivalent to a single rod of length L moving at constant velocity v_0 in the fluid in a direction parallel to its long axis. In that case, the velocity field for distances $r \ll L$ has only a weak logarithmic dependence of r, meaning that up to a correction of order $\ln(L/a)$, the velocity field is only weakly dependent on distance and for most practical cases will differ by less than an order of magnitude from v_0. Here we take the velocity of the fluid, $v(r)$, to go to zero far from the rod. This is related to the well known result that the drag on a rod of length L will only differ by a logarithmic factor from that of a sphere of diameter L despite the latter's much greater volume [18]. Such a system of densely packed impellers would be very efficient at driving the motion of surrounding fluid.

Now consider the more realistic case in which the impeller size is less than the spacing between them, which is much less than the length of a microtubule, that is $a < d \ll L$. At a distance $r \gg d$, the velocity field will behave just as in the closed-packed case except appear to have a diminished impeller velocity. That is for $d \ll r \ll L$, the magnitude of the velocity $v(r) = v_0 f(a/d) g(r)$, where $g(r)$ contains all the distance dependence of the velocity field, and $f(a/d)$ is how the velocity scales with the ratio of a/d. In the limit where a/d is very small, the velocity between impellers will decay to zero. We recover the motion of isolated impellers in this case, where it is well known (e.g. Stokes' drag) that the velocity field is proportional to a. Therefore for small argument $x(= a/d)$, $f(x)$ is linear (in other words, the fluid velocity is proportional to a.) Using this general argument we conclude that, independent of the exact shape of the impellers, the flow velocity is reduced from the closed-packed case by a factor $\sim a/d$. The effect of the impellers only starts decreasing substantially at a distance of order the length of the microtubule, L, below which it should only have a weak logarithmic dependence. In other words, for a spherical region just enveloping a

microtubule, the fluid velocity is slowly varying and reduced from the kinesin motor velocity by a factor of order a/d. The above arguments suggest that only a low density of microtubules would be needed for cytoplasmic streaming. We will analyze the case of many microtubules below.

The above analysis only pertains to a single isolated microtubule. Because of the long range nature of the hydrodynamic interaction, the behavior of many microtubules will be quite different. Below we find that the consideration of many further enhances the streaming capablities of this system. To understand how this affects the above analysis, consider all space filled with an infinite forest of microtubules, all oriented in the same direction. First if we ignore the microtubules and just consider the spherical impellers, then if we move to a reference frame moving with the impeller velocity, the system is static and the velocity everywhere is zero. Therefore in the original reference frame, the fluid is also moving uniformly at the impeller velocity. This is not correct because we have ignored the hydrodynamic drag of the microtubules represented by the line going through the spheres in Fig. S1. To estimate their effect on the fluid velocity, we denote the drag coefficient on an impeller by b_I and that of a section of microtubule length d by b_M. Then we go to a reference frame velocity v such that the total force acting on the combined system of impellers and microtubules is zero, so that $b_I(v_0 - v) - b_M v = 0$, or $v = b_I v_0/(b_I + b_M)$. Because the net force acting on this system is zero in this frame, v is the velocity of the fluid far from the microtubules. Of course close to each microtubule, the velocity will differ from the value far away, but this will only affect points that are within a distance $a + d$ from the microtubule. If we assume conservatively, that the impellers are very thin cylindrical sheaths, fitting right over the microtubules, then this speed is $v_0 a/d$. If the hydrodynamic radius of the impellers is larger than such a model, then the velocity will be larger. The exact formula depends on the shape of the impellers. This argument assumes an infinite volume of microtubules but the corrections to this due to the finite nature of the system are not important for the estimates we are making.

3 Necessity of microtubule contact

The question of whether or not free floating microtubules with kinesin-driven impellers contribute to force generation for streaming is important. Our photobleaching tests demonstrate that there is a subcortical layer of microtubules that is stationary relative to the cortex, while subcortical cytoplasm streams past (Fig. 7 and Movie S7). In this case, the principle of Newton's third law dictates that the force on cytoplasmic fluid from plus-end directed kinesin-impeller movement is matched by an opposite force on microtubules that is transferred through the cortex to the surrounding tissues of the egg chamber and whatever it is attached too. Thus the impellers and fluid move while the microtubules do not, other than sinusoidal bending around their tethered minus ends. Could free microtubules deeper within the oocyte also drive flow? In this case, the force from kinesin-driven impellers on a microtubule will cause the microtubule to move with its minus-end leading, opposite the direction of the impellers. Because the force is equal in both directions, the motion imparted to cytoplasmic fluid must be equal in both directions. The result is that the microtubule will move one way, the impellers will move the other and, beyond very local displacements, the cytoplasm will not move.

From a more physical perspective, a free floating microtubule with kinesin moving on it will apply *zero* net force to the fluid. This is a simple consequence of Newton's third law, or equivalently, conservation of momentum. Consider a dumbell shaped machine with two spheres of different radii connected by a spring. Starting with the dumbell in a compressed state and then letting it go will impart equal and opposite forces on the two spheres, independent of their radii. Immersed in a viscous fluid, it is the total force that acts on a sphere that determines the velocity field of its surrounding fluid at large distances (see Eq. S-28). The fact that the small sphere travels a greater distance than the large one is irrelevant; they both impart equal and opposite forces to the fluid, so the net fluid movement at large distances is zero. This is analogous to the zero total charge on a dipolar object in electrostatics. Equal and opposite forces in a fluid imply dipolar fluid motion at large distances, which decays rapidly.

This does not contradict the fact that bacteria are able to swim: the force propelling the bacterium forward is countered by an equal and opposite force on the environment, leading to velocity fields that are dipolar at large distances, but still allowing motion of the bacterium due to local fluid displacement [19]. In the case analyzed above where kinesin is attached to microtubules, we have taken the microtubules to be static, and therefore momentum can be transfered between kinesin and microtubules, which will transfer the momentum through the oocyte cortex and membrane to the outside environment. When we consider the motion of microtubules, it is therefore important to have one end connected to the cortex to allow momentum transfer from the outside surroundings of the oocyte to the cytoplasm. Without such a microtubule connection to an external system, the motion of kinesin cannot lead to long range hydrodynamic motion of the fluid and will not lead to efficient cytoplasmic streaming by relatively few motor proteins. Contact with the cortex is therefore crucial, as it allows for transfer of force from the outside of the oocyte to the cytoplasm, enabling fast streaming of a large volume of cytoplasmic fluid to be powered by a much smaller volume of kinesin driven impellers.

4 Mathematical analysis of microtubule bending due to kinesin forces

During fast streaming, microtubules are largely aligned with each other and the local fluid motion, but they do exhibit chaotic wavelike bending motions. We begin with the equation for a single microtubule with an applied force tangent to the direction of the chain due to kinesin driving impellers toward the plus end. The position of the microtubule at arclength s and at time t is denoted $\mathbf{r}(s,t)$. As is usual at small scales, all inertial effects are negligible and the system is dominated by the drag coefficient per unit length ν,

$$\nu\frac{\partial \mathbf{r}}{\partial t} = -C\frac{\partial^4 \mathbf{r}}{\partial s^4} + \frac{\partial}{\partial s}(T(s)\frac{\partial \mathbf{r}}{\partial s}) - f_k\frac{\partial \mathbf{r}}{\partial s} + \nu v\hat{k}. \tag{S-1}$$

C denotes the elastic bending constant of the microtubule. The tension $T(s)$ enforces the inextensibility of microtubules which can be written as $|\partial \mathbf{r}/\partial s| = 1$. This is the three dimensional version of a two dimensional equation used to model rotating spiral patterns seen in motility assays [28] where we have added the extra term $\nu v\hat{k}$ discussed below.

Kinesin motors walking along the microtubule are assumed to be carrying cargoes that push on the cytoplasmic fluid that surrounds them. By Newton's third law, this force is matched by an equal and opposite force on the microtubule. Assuming a high density of kinesin, the effective force on the microtubule will be in the direction of the local tangent to $\mathbf{r}(s)$ which is $\partial \mathbf{r}/\partial s$. The coefficient f_k gives the strength of the force. Lastly we add a uniform flow field representing the velocity of the cytoplasm v in the vicinity of the microtubule which we take to be in the $\hat{k}$ direction.

We rescale to dimensionless variables

$$\sigma = s/\rho_0,\ \mathbf{U} = \mathbf{r}/\rho_0,\ \tau = t\omega_0,\ T' = T\rho_0^2/C,\ \text{and}\ h = \nu v/f_k \tag{S-2}$$

so that

$$\frac{\partial \mathbf{U}}{\partial \tau} = -\frac{\partial^4 \mathbf{U}}{\partial \sigma^4} + \frac{\partial}{\partial \sigma}(T'(\sigma)\frac{\partial \mathbf{U}}{\partial \sigma}) - \frac{\partial \mathbf{U}}{\partial \sigma} + h\hat{k}. \tag{S-3}$$

This requires that

$$\omega_0 = f_k/(\nu\rho_0),\ \text{and}\ \rho_0^3 = C/f_k. \tag{S-4}$$

ρ_0 and ω_0 are constants that make our new variables dimensionless.

We will consider solutions where the minus end is tethered to a point, say the origin, so that $\mathbf{r}(s = 0, t) = 0$ and is freely hinged at that point. The plus end is free. The total arclength of the microtubule is denoted by L. The general characteristic of all numerical solutions to Eq. S-1 is that for large s the solutions appear to be traveling waves. In fact, the form of solution becomes independent of L so in fact we could consider this problem in the limit $L \to \infty$. For example we find solutions that asymptotically become helical with a fixed path and radius for large s. Other solutions are planar and are periodic in s. In all these cases the solution has the form of a travelling wave that we analyze in detail below.

4.1 Steady State Travelling Wave Solutions

Now we look for steady state travelling wave solutions. First we clarify what this means; the whole microtubule should not be translating because the minus end, (far away from where the travelling wave solution is valid) is tethered. The position averaged over one period of a filament subunit, $\langle \mathbf{U} \rangle$, should be time independent. If the microtubule is stretched out in one particular direction, there should be a displacement $\mathbf{U}_d$ of the microtubule about a straight line solution, so we can look for solutions of the form

$$\mathbf{U}(\sigma, \tau) = \mathbf{U}_d(\sigma - v_d\tau) + \alpha\sigma\hat{k}. \tag{S-5}$$

The term $\mathbf{U}_d$ describes a transverse displacement waveform that travels along the backbone of the chain at velocity v_d, maintaining its shape. Here α is the extent to which the chain is extended in the direction of the fluild motion. Therefore we require

$$\frac{\partial \langle \mathbf{U}_d \rangle}{\partial \sigma} = 0 \tag{S-6}$$

where the average is taken over the argument $\sigma - v_d\tau$.

Since $\mathbf{U}_d$ is transverse, α sets the relation between σ and the z-axis ($\hat{k}$), such that $v_z = \alpha v_d$. If we choose $v_d = 1$ and in addition $\alpha = h$, we should obtain solutions that propagate along the fluid direction with the same unitless velocity as the fluid motion. Looking back to our original units, $v_d = 1$ corresponds to a wave propagating along the backbone of the chain at velocity f_k/ν (roughly the kinesin walking speed). Recall that h is the rescaled unitless velocity of the external flow field, so $\alpha = h$ is the condition that the traveling wave form should propagate along the axis aligned with the globally imposed fluid velocity at the same speed as the fluid. This will allow us to look for configurations that are stationary along that axis in the frame of the fluid.

Substituting Eq. S-5 into Eq. S-3 gives a left hand side of $-v_d\partial\mathbf{U}_d/\partial\sigma$ and a term of the form $-\partial\mathbf{U}_d/\partial\sigma$ on the right hand side, simplifying the equation to

$$\frac{\partial^4 \mathbf{U}}{\partial \sigma^4} + \frac{\partial}{\partial \sigma}(T'(\sigma)\frac{\partial \mathbf{U}}{\partial \sigma}) = 0. \tag{S-7}$$

We define $\mathbf{w} = \partial \mathbf{U}/\partial\sigma$ and note that the inextensibility requirement $|\partial \mathbf{r}/\partial s| = 1$ implies that $|\mathbf{w}| = 1$. We can write

$$\mathbf{w} = \frac{\partial \mathbf{U}_d}{\partial \sigma} + \alpha \hat{k} \tag{S-8}$$

Note that $\mathbf{w}(\sigma, \tau)$ depends only on $\sigma - \tau$. Because $\mathbf{w}$ is a function of only one variable $\xi \equiv \sigma - \tau$, we can integrate Eq. S-7 with respect to ξ obtaining

$$\frac{d^2\mathbf{w}}{d\xi^2} - T'(\sigma)\mathbf{w} = -g\hat{k}. \tag{S-9}$$

The integration constant on the right hand side $-g\hat{k}$ must lie in the $\hat{k}$ direction by symmetry. This is the same equation as that of the classical mechanics of a particle of unit mass, with position $\mathbf{w}$ travelling on the surface of a unit sphere under the influence of gravity, with the variable ξ being analogous to time. The term $-T'$ is a normal force that constrains the particle to stay on the sphere's surface.

From Eq. S-6 and Eq. S-8 we see that the motion is subject to the constraint

$$\langle \mathbf{w} \rangle = \alpha \hat{k} \tag{S-10}$$

The constant g and the initial conditions of the particle must be chosen so as to satisfy this constraint. There are an infinite number of solutions satisfying these conditions leading to different steady state solutions for the microtubule.

The spherical pendulum Eq. S-9 has been analyzed [S3] in detail. In general the orbits will not be closed, but we will relegate our discussion below to two cases where this is the case, circular motion in Eq. S-9, corresponding to helical conformations of a microtubule, and motion in the $x - z$ plane. The latter case is important when we introduce a hard wall, with the z axis being the direction of the global fluid field, and the solutions give shapes similar to cycloids.

4.2 Scale Invariant Family of Solutions

One important point to notice about the general structure of Eq. S-9 is its invariance under change of ξ, that is $\xi \to \lambda\xi$. A change in scale of λ does not modify the solution, because $T'(\xi)$ and g are

both constraints, and can therefore be chosen arbitrarily. So that if $\mathbf{w}(\xi)$ is a solution to Eq. S-9, so is $\mathbf{w}(\lambda\xi)$. Furthermore all solutions of this form will have the same $\langle\mathbf{w}\rangle$ and hence the same α. Note that a length scale shift of $\mathbf{w} = \mathbf{w}_0(\lambda\xi)$ corresponds to a displacement of $\mathbf{U} = (1/\lambda)\mathbf{U}_0(\lambda\xi)$, which changes scale because of the $1/\lambda$ prefactor in this expression. This means that for every steady state conformation of the microtubule, there exists a family of steady state solutions with identical shape but arbitrary size.

4.3 Circular Orbits

Circular orbits are solutions to Eq. S-9. Eq. S-10 requires that the vertical height of the orbit be at $w_z = \alpha$. Therefore the radius perpendicular to the global fluid velocity $\hat{k}$ (the w_x, w_y plane) is

$$w_\perp \equiv \sqrt{1-\alpha^2}. \tag{S-11}$$

It is first easiest to analyze this by direct analogy to the classical mechanical problem of a unit mass particle moving on a unit sphere (the spherical pendulum). If the height above the sphere is α, then application of Newton's laws gives that the tension must balance the force of gravity g and the centripetal acceleration $v^2/w_\perp$ giving

$$\frac{g}{v^2} \equiv \frac{\alpha}{1-\alpha^2} \tag{S-12}$$

Where v is not the real velocity of the microtubule but $|d\mathbf{w}_\perp/d\xi|$. This is the rate at which the tangent vector rotates in the $x-y$ plane (the plane perpendicular to the fluid motion). Because $|d\mathbf{U}_d/d\xi| = |\mathbf{w}_d| = r_c$ is a constant, $\mathbf{w}_d$ is a circle. Therefore according to Eq. S-5, this will give a helical conformation of the microtubule.

In the spherical pendulum analogy, the angular velocity of the particle is $\Omega_p = v/w_\perp$. The total arclength of the chain (in dimensionless units) of a single period of the chain is

$$S = \frac{2\pi R}{\sqrt{1-\alpha^2}} \tag{S-13}$$

and $S\Omega_p = 2\pi$ so that $S = 2\pi/\Omega_p = w_\perp/v$. Comparing this with Eq. S-13 we obtain

$$R = \frac{w_\perp}{v}\sqrt{1-\alpha^2}. \tag{S-14}$$

Using Eq. S-11 this gives

$$R = \frac{1-\alpha^2}{|\frac{dw_\perp}{d\xi}|} = \frac{1-\alpha^2}{v} \tag{S-15}$$

Because g is a free parameter, v can be any positive number and therefore Eq. S-15 implies that the radius of the helix can be arbitrary.

Because the velocity of this travelling wave is unity, the spatial and temporal periodicities are equal. Therefore the period of rotation of the helix P' is equal to S in Eq. S-13, in the dimensionless units that we are using. Therefore the relationship between the period and the pitch is

$$P' = \frac{2\pi R}{\sqrt{1-\alpha^2}} \tag{S-16}$$

In terms of our original units the period is

$$P = \frac{2\pi R\nu}{f_k\sqrt{1-\alpha^2}} \tag{S-17}$$

4.4 Two Dimensional Solutions

As we will see in Sec. 4.5, the presence of a wall often causes conformations to become flat, that is two dimensional. Therefore it is of interest to analyze this case. We consider orbits in the $x-z$ plane. This corresponds to a pendulum swinging around vertically through the bottom of the sphere. This is a standard introductory mechanics problem. Letting θ denote the angle with respect to the $-\hat{k}$ direction,

$$\ddot{\theta} = -g\sin\theta \tag{S-18}$$

where the dots that normally represent a time derivative are really derivatives with respect to ξ. Low energy solutions where the total energy E is less than g give θ oscillating between two bounds. In this case the curve for the microtubule will look sinusoidal. Beyond the separatrix where $E > g$,

θ will increase without bound. This gives rise to microtubule conformations that look close to prolate cycloids. In other words, the microtubule forms a travelling wave that periodically loops backwards (Fig. S2).

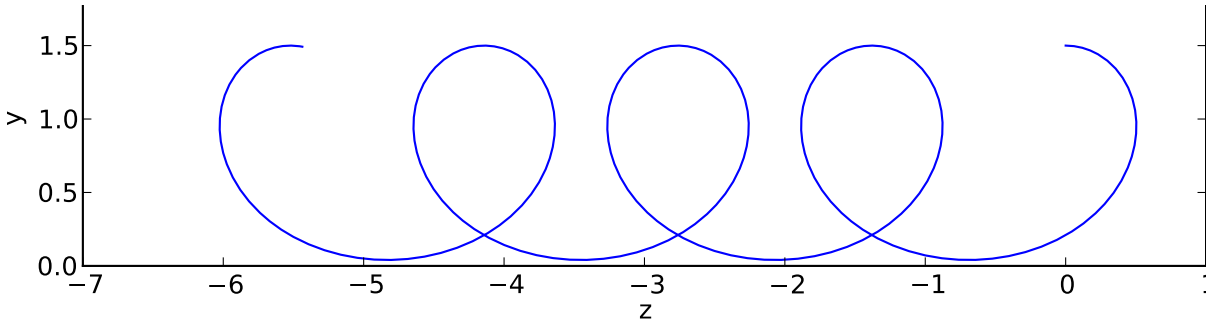

Figure S2: A two dimensional travelling wave solution for a microtubule that looks close to a prolate cycloid but differs from it in functional form.

Small values of $|\alpha|$ correspond to low values of g/E. In this case, the particle spends almost equal times at all points on the circle giving a small value of $\langle w \rangle = \alpha$. As g/E increases to 1, α increases and the loops become tighter; a situation that is very costly energetically. However this is not the only solution to these equations for a fixed value of α. If instead we consider solutions with $E < g$, then large g/E corresponds to small oscillations of $\mathbf{w}$ about $-\hat{k}$. In this case, $|\alpha|$ is close to 1 and the curve has no tight loops. The shape of the microtubule is close to a sine wave.

To obtain the relationship between $G \equiv g/E$ and α we use conservation of energy to obtain the period,

$$\dot{\theta} = \sqrt{2E(1 + G\cos\theta)} \tag{S-19}$$

The time average of $\mathbf{w}$ in the $\hat{k}$ direction is

$$\langle \cos\theta \rangle = \frac{\int_0^\pi \frac{\cos\theta}{\sqrt{1+G\cos\theta)}} d\theta}{\int_0^\pi \frac{1}{\sqrt{1+G\cos\theta)}} d\theta} \tag{S-20}$$

This can be expressed in terms of elliptic integrals as

$$\langle \cos\theta \rangle = \frac{1}{G}(1 - (1+G)\frac{\mathsf{E}(2G/(1+G))}{\mathsf{K}(2G/(1+G))}) \tag{S-21}$$

Where E and K are the complete Elliptic integrals of the first and second kind respectively. For bounded orbits, below the separatrix, the corresponding expression can be calculated giving

$$\langle \cos\theta \rangle = -2\frac{\mathsf{E}(\frac{e+1}{2})}{\mathsf{K}(\frac{e+1}{2})}) + 1 \tag{S-22}$$

A plot of the $\alpha = \langle \cos\theta \rangle$ versus $1/G = E/g$ is shown in Fig. S3 using these two expressions. $\alpha \to 0$ in the limit as $G \to 0$. Note that there are two possible values of E/g corresponding to one value of positive α.

The case of $\alpha = 0$ corresponds to the case of circular orbits discussed in Sec. 4.3. The cytoplasmic streaming velocity is $\propto h$ (see Eq. S-3). When $h = 0$, we have shown that the solutions are circular. If h is now made very small, we expect that the solution will only be slightly perturbed from circular solutions. This corresponds to a small value of g/E. Therefore the value of G that is chosen for small enough h should correspond to the larger value of $1/G$ shown in Fig. S3. This corresponds to almost circular loops shifting slightly forward after every turn. As h increases, the loops become tighter giving rise to a high elastic bending energy. At some point therefore, we expect a transition to another state. In fact, simulations discussed in Sec. 4.6 show that near a flat surface, the microtubule transitions out of the plane to a helical shape at $h \approx .385$ for 128 links in a chain. For still larger h, the microtubule becomes flat again looking close to sinusoidal.

4.5 Numerical Implementation of the Full Solutions

By comparing the steady state solutions found above for large arclength s and time t, we will see that these solutions are physically realistic ones to consider. As we will see, the full equations of motions go to solutions of this type. However this is not a complete description of the problem, because of these solutions a particular one is selected from a whole family of solutions. The same behavior occurs in other problems in pattern selection such as dendritic growth [S4, S5].

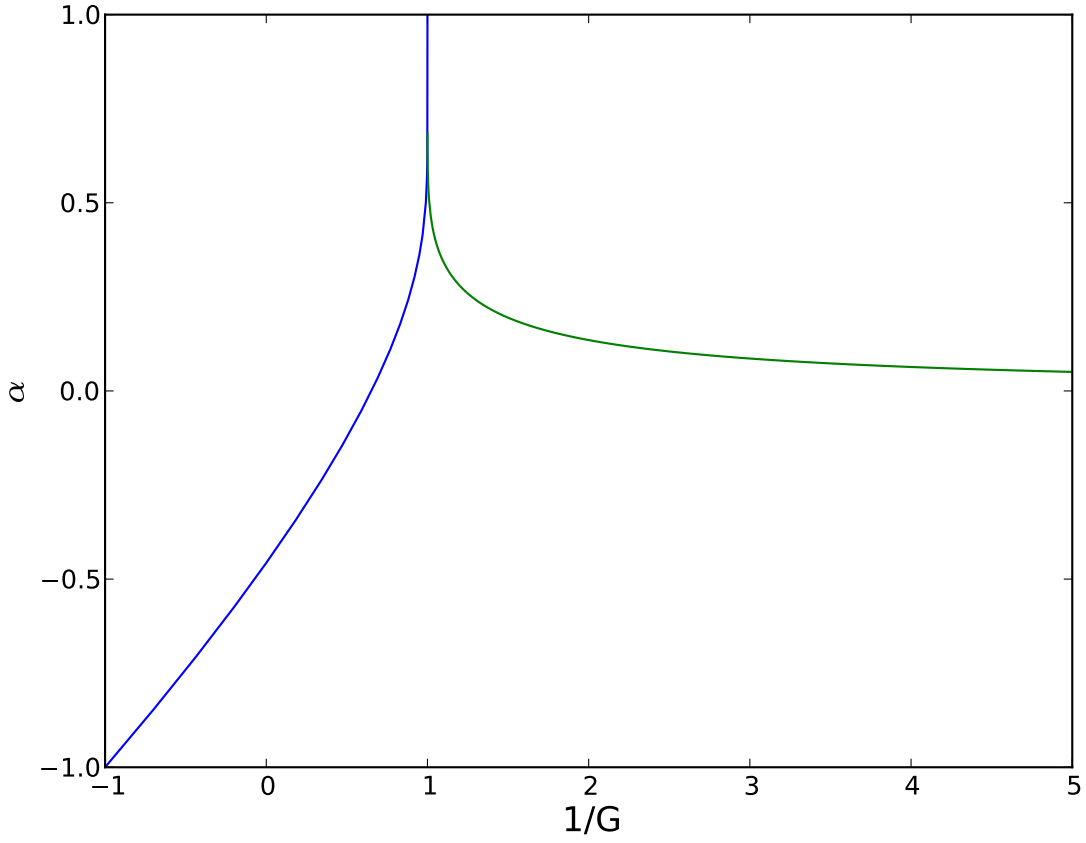

Figure S3: A plot of the value of α, the wave propagation velocity, as a function of $1/G$, which is the energy of the analogous spherical pendulum.

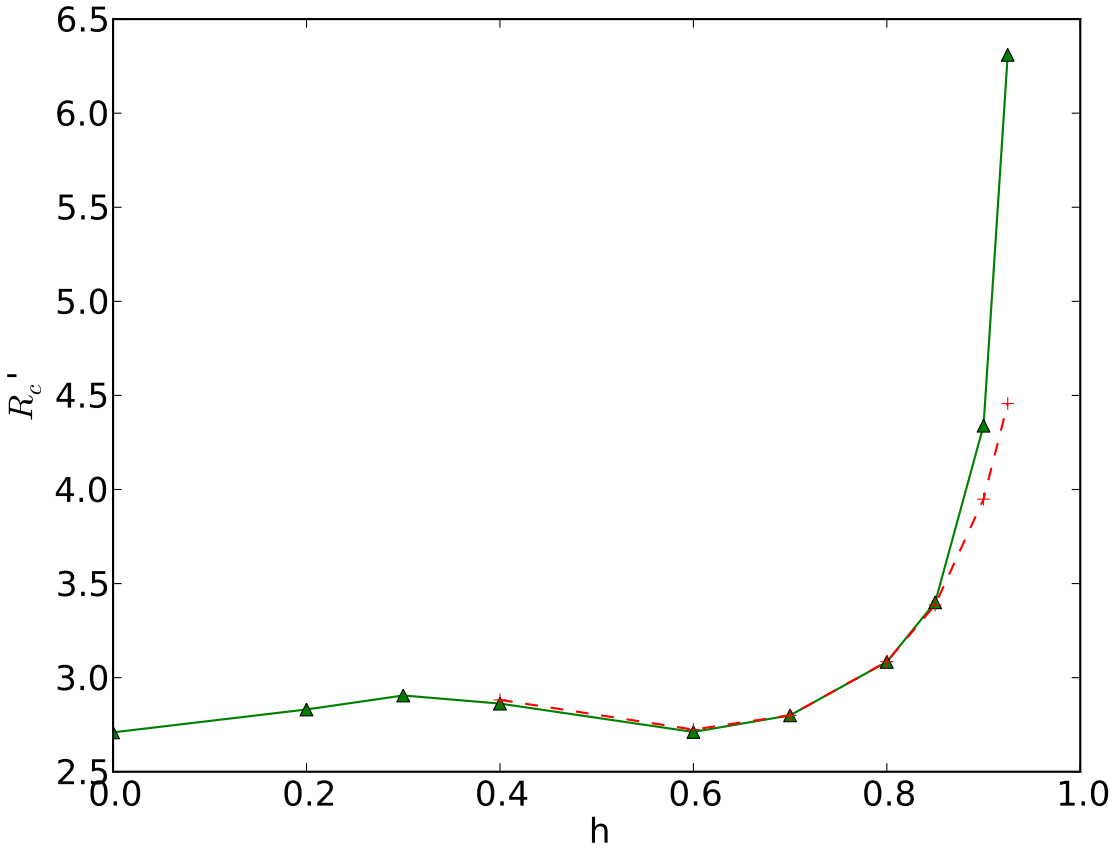

Figure S4: The rescaled radius of curvature for the helical configuration, R_c/ρ_0, versus the rescaled fluid velocity field $h = \alpha$. The green triangles are for 64 link chains, the red + symbols are for chains of 128 links.

4.6 Comparison With Simulation

Eq. S-1 was analyzed numerically using a method similar to that used in the context of gel electrophoresis [S6, S7]. Link length drift was handled using a similar procedure to that implemented for chains with inertia [S8] One end was constrained to have coordinates at the origin, while the

other was free.

A Runge Kutta time step was 0.001, with the elastic bending coefficient $C = 20$, the kinesin force magnitude $f_k = 2$ and simulations were performed with $N = 64$ or $N = 128$ links, as will be noted below. The units are such that the distance between links is set to unity, and the friction coefficient ν, which determines the units of time, is also set to 1.

We first consider the case of a microtubule with no wall or other external forces aside from the external velocity field. As a function of the rescaled external velocity field h, the radius of curvature and period were calculated once the system had reached steady state. Using rescaled variables as defined by Eqs. S-2 and S-4 we can write the dimensionless radius of curvature as $R_c' = R_c/\rho_0$, and the dimensionless period as $P' = \omega P$. The radius of curvature was calculated at the middle of the chain to reduce finite size effects. The results are shown in Figs. S4 and S5. The data for R_c, Fig. S4 using 64 links, is very close to those of 128 links except for the highest h values. The data for the period, Fig. S5(a) show good agreement for both chain sizes at all values of h studied.

We now test the analytic predictions that we made relating the period to the radius of the helix and α given by Eq. S-16, and our conclusion that $\alpha = h$. The relationship between the radius of curvature R_c and the radius R of the helix is readily calculated to be $R = R_c(1 - \alpha^2)$. Therefore Eq. S-16 gives

$$P' = 2\pi R_c' \sqrt{1 - \alpha^2} \tag{S-23}$$

With this prediction, and using the data for R_c in Fig. S4, we can independently calculate P' for 64 link chains. We can only do this where finite size effects are not important and therefore omit the highest two h values from this analysis. The data, Fig. S5(b), show excellent agreement to within the differences expected by finite size effects. This corroborates our analytical analysis of steady state solutions.

The case of $h = \alpha = 0$ displayed in Fig. S4 can be written in terms of the original dimensional variables of Eq. S-1 using Eq. S-4

$$\nu R\omega / f_k = 1. \tag{S-24}$$

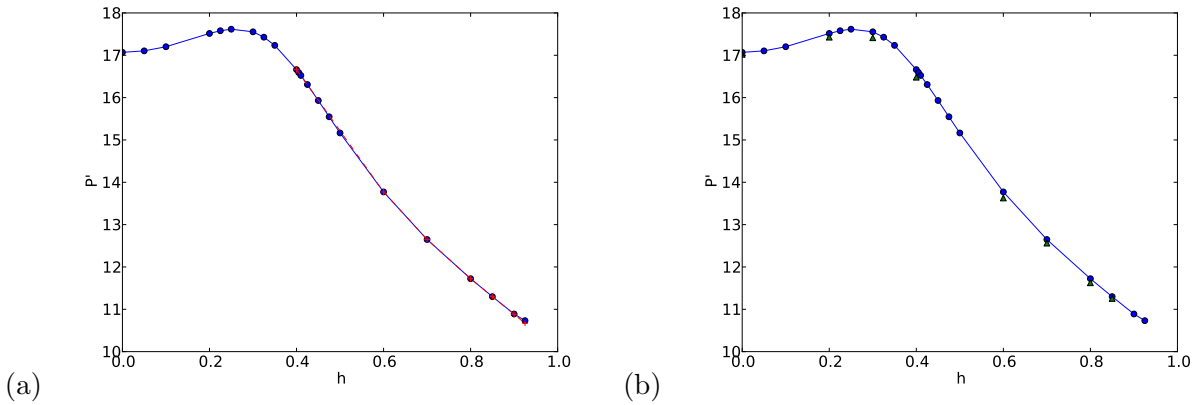

Figure S5: (a)The rescaled period $P' = P\omega$ versus the rescaled velocity field $h = \alpha$. The blue circles are for 64 link chains, the red + symbols are for chains of 128 links. Here the period is measured directly by timing repeated motion. The line is a guide for the eye. (b) The rescaled period $P' = P\omega$ versus the rescaled velocity field $h = \alpha$ calculated by using Eq. S-23 and data on the radius of the helix versus h shown in Fig. S4. The result is shown by the green triangles. The blue circles are the same data shown in Fig. S5(a) by directly measuring the period, which shows good agreement with the numbers produced by using Eq. S-23. Again the line is a guide for the eye.

And using our numeric solutions we can obtain.

$$R_c = (C/(\beta f_k))^{1/3}. \tag{S-25}$$

From the numerical solution, this gives $\beta = 0.05 \pm 0.0005$. This is useful in analyzing experimental data, as R_c is nearly constant for $h < 0.7$.

Next we consider the presence of a wall. We introduced a force representing a wall in the $y - z$ plane of the form

$$\mathbf{f}_w = \frac{x^2}{(x+1)^2}\hat{i} \tag{S-26}$$

which is only present for $x < 0$. The force is singular at $x = -1$ preventing the chain from crossing that plane. The period as a function of h is shown in Fig. S6 for $C = 20$ and chains with 128 links.

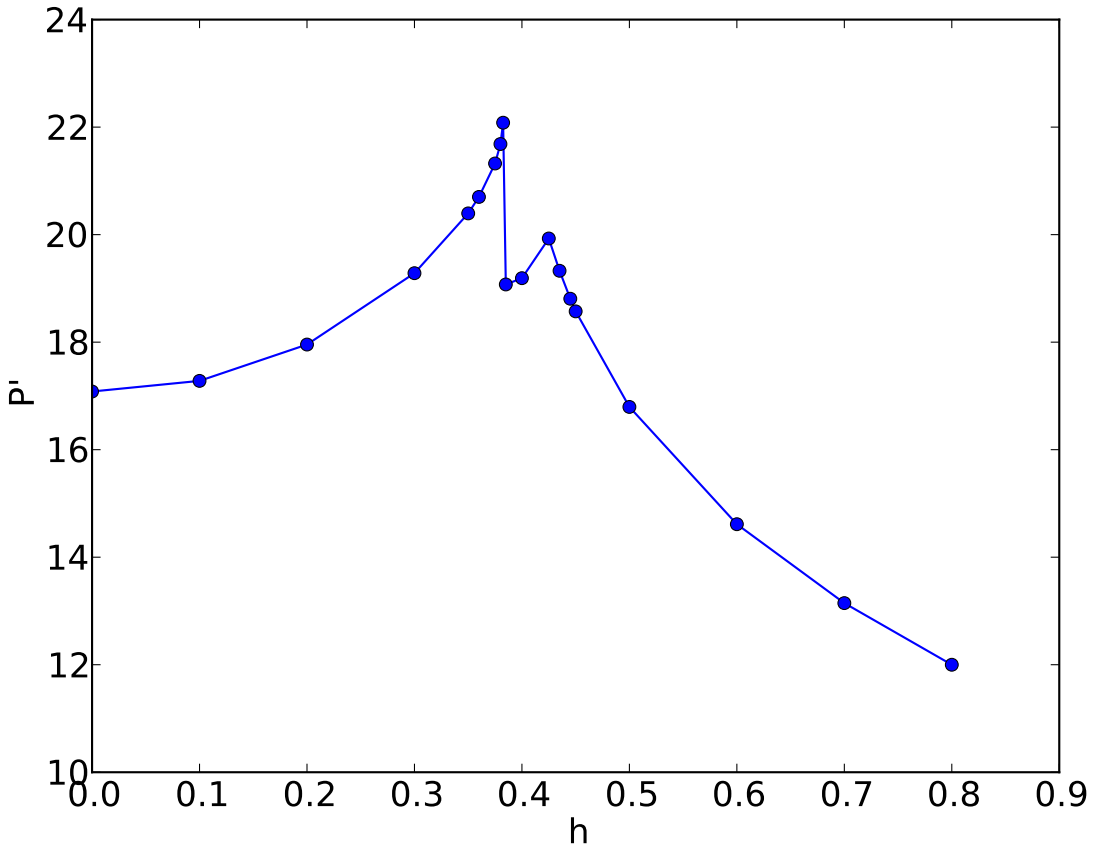

Figure S6: The rescaled period $P' = P\omega$ versus the rescaled velocity field $h = \alpha$ for chains of 128 links.

For small values of h, the period does not vary much. The shapes obtained are flat and appear to be the same as those found in Sec. 4.4. However there is non-analytic behavior at $h \approx 0.385$

corresponding to a transition to flattened helical waves. Then at $h \approx 0.425$ the solution becomes almost completely flat and showing waves that look closer to sine waves, corresponding to the flat sinusoidal-like solutions studied in Sec. 4.4.

We now consider the dependence of period and curvature on the length of chains L. Our analytical solutions have been in the limit that the chain length $L \to \infty$. For finite length chains, we expect corrections to this behavior. In this case we consider $h = 0$ and study how the rotating spiral wave solutions vary with increasing length. Fig. S7(a) shows the dependence of the radius of curvature measured halfway along the arclength, as a function of chain length. As usual, the rescaled dimensionless variables, see Eqs. S-2 and S-4 have been used. The curve shows a non-monotonic dependence on L that levels off at $L \approx 20$. Fig. S7(b) shows that the rescaled period is slightly non-monotonic as well but decreases to a constant value at $L \approx 15$.

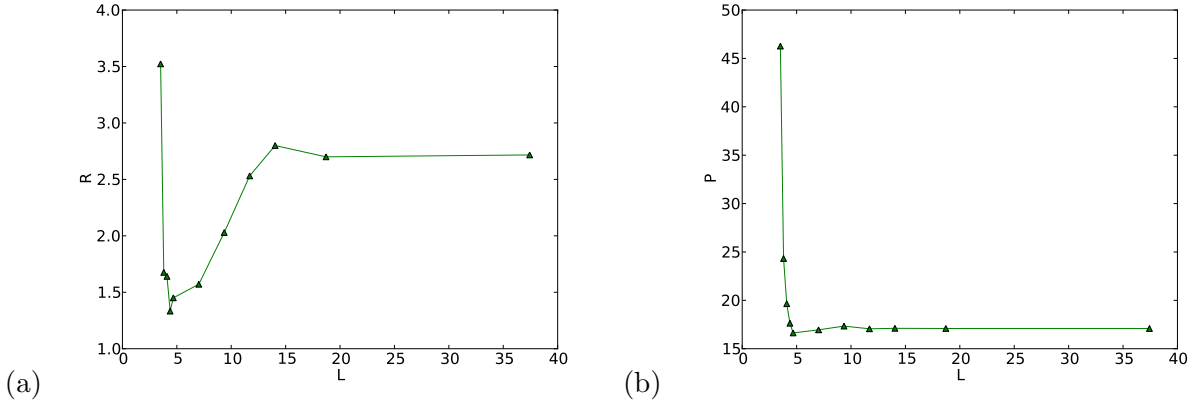

Figure S7: (a) The rescaled radius of curvature measured at the middle link of a chain versus the rescaled chain length in steady state for $h = 0$. (b) The rescaled period versus the rescaled chain length in steady state for $h = 0$.

Note that in Fig. S7(b) the period diverges for finite $L \approx 3$. Below this point, the solution is a static straight line. This is similar to the usual buckling transition for a finite length elastic rod [S9]. Thus the microtubule needs to be sufficiently long to undergo the dynamical instability

analyzed here.

4.6.1 Selection of Scale

As noted in Sec. 4.2, there exists a continuous family of steady state solutions because if $\mathbf{w}(\xi)$ is a solution, then so is $\mathbf{w}(\lambda\xi)$ for arbitrary λ. The general way that a particular value of λ is selected is likely to be due to the same mechanism as in other pattern formation problems [S4, S5]. The travelling wave solutions ignore the boundary conditions at the ends $s = 0$ and $s = L$. Far from those ends, we have found a continuous family of solutions. However these solutions become invalid close to the ends. The travelling wave solutions are only valid in the limit of $0 << s << L$. The full solution must match to one of these travelling solutions in that region but will differ greatly near the ends.

As an example, consider the circular solutions of Sec. 4.3 with $h = \alpha = v = 0$. There the steady state solution is a rotating circle wrapped around on itself of *arbitrary radius* R. However near the end $s = 0$, the solution goes into the circle's center. Similarly it deviates from a circle at $s = L$. In analogy with other pattern growth problems such as the "Geometric Model" [S4], where the mathematics have been analyzed in detail, we expect that the boundary conditions imposed on the ends, will only be satisfied for certain values of R. If there is more than one allowed value of R, the value picked out will be the most stable of these. In the Geometric Model the form of the equations is much simpler, making it possible to understand the overall structure of the problem more easily. In the present case, a precise understanding of the numerical results will be the subject of future research.

5 Fluid Mediated Polymer Interactions

After the foregoing analysis of the dynamics of individual polymers in an externally imposed flow field, we now investigate how such a flow field could actually be generated internally by kinesin forces acting on a large group of microtubules. To produce a global flow field in the fluid, we need a

large number of microtubules all aligned and contributing to the driving of the field in a correlated manner. In addition to investigating steady state values, the behavior with small kinesin forces could determine criteria under which spontaneous global velocity field formation could occur. To do these types of calculations, a more detailed view of the interaction between elements in the system needs to be taken.

5.1 Introduction to the Oseen Tensor

Since streaming occurs in a low Reynolds number regime, the motion of the fluid is described by the simplified Stokes equations:

$$\begin{aligned} \nabla p &= \mu \nabla^2 \mathbf{u} + \mathbf{f} \\ \nabla \cdot \mathbf{u} &= 0 \end{aligned} \tag{S-27}$$

The linearity of the Stokes equations allows for solutions to be obtained via a Green's Function, such that for a continuous force density $\mathbf{f}(\mathbf{r})$,

$$\begin{aligned} \mathbf{u}(\mathbf{r}) &= \int \mathbf{f}(\mathbf{r}') \cdot \mathbf{J}(\mathbf{r} - \mathbf{r}') d\mathbf{r}' \\ p(\mathbf{r}) &= \int \tfrac{\mathbf{f}(\mathbf{r}') \cdot (\mathbf{r} - \mathbf{r}')}{4\pi |\mathbf{r} - \mathbf{r}'|^3} d\mathbf{r}' \end{aligned} \tag{S-28}$$

Where

$$\mathbf{J}(\mathbf{r}) = \frac{1}{8\pi\mu} \left(\frac{I}{|\mathbf{r}|} + \frac{\mathbf{r}\mathbf{r}^T}{|\mathbf{r}^3|} \right) \tag{S-29}$$

is a second rank tensor field known as the Oseen Tensor. The Oseen tensor has had great success in describing how small or thin objects interact in fluid, as well as the self interaction of polymers. When used to describe the effect of applying force to a very small sphere of radius a, the Oseen tensor has higher order corrections in $a/\mathbf{r}$, where $\mathbf{r}$ is the distance from the sphere, but these begin at $(a/\mathbf{r})^3$ and should not play a significant role in cross polymer interactions. Of particular interest is its use in modeling polymers as a long chain of beads, which will lend itself well to numerical simulation.

5.2 Model for Hydrodynamic Interactions

For this multi-filament model, we are going to use the same structure for the microtubule as for the solitary case. This models the microtubule as a chain of beads with some tension T and stiffness parameter C. The equation of motion for each microtubule in the array is modified now by the inclusion of the Oseen interaction tensor. Each microtubule and its kinesin-driven impellers are in direct contact with the fluid and at the interface the velocity of the fluid must match the velocity of the objects suspended in it. This means that any force exerted on the objects will also be transmitted to the fluid locally. These forces form the force density used in the Oseen tensor to determine the fluid velocity in all of space, which will also determine the motion of the microtubule and impeller system.

This is a bit more complex than simply adding the tensor to the previous equation of motion, as the interaction tensor needs to include the forces of all objects moving in the fluid. Previously, we simply included the kinesin as a force tangent to the backbone of the microtubule, and while that is still going to be our model, we now need to include consideration for the reaction force produced against the impeller, as this will be transmitted back to the microtubule by the long range hydrodynamic forces.

In order to determine the effect that this extra force density will have on the dynamics, we need to be more explicit with the configuration of the impellers. Consider the impellers of largest dimension q to be attached to the microtubule by kinesin motors with no side being preferred at a characteristic distance a with, as in the single microtubule consideration, $a < q \ll L$, with L again being the microtubule length. We can consider this to form a uniform density of impellers around the microtubule, and the kinesin motors cause the impeller and the microtubule to move relative to each other with a fixed velocity in the direction of the tangent of the microtubule backbone.

The fluid velocity field can now be computed by applying the Oseen tensor and integrating over the force densities present in the system. The forces acting on the microtubule can be integrated by integrating over the backbone of the chain. The forces acting on the impellers can be computed

by integrating over a cylindrical sheath around the microtubule, giving us

$$\mathbf{u}(\mathbf{r}) = \int \left[\mathbf{J}(\mathbf{r} - \mathbf{r}'(s))[-C\frac{\partial^4 \mathbf{r}'}{\partial s^4} + \frac{\partial}{\partial s}(T(s)\frac{\partial \mathbf{r}'}{\partial s}) - \mathbf{f_k}] + \int \mathbf{J}(\mathbf{r} - \mathbf{r}'(s) + \mathbf{a}(s))\frac{\mathbf{f_k}}{2\pi|\mathbf{a}|}\frac{\partial \mathbf{r}'}{\partial s} d\hat{\mathbf{a}} \right] ds \tag{S-30}$$

where $\mathbf{u}$ is the fluid velocity and $\mathbf{a}$ is a vector pointing radially outward from the microtubule axis to the impeller location. Recall that C, $T(s)$, and $\mathbf{f_k}$ are the microtubule stiffness parameter, microtubule tension, and kinesin walk force respectively. Because the microtubule system is in contact with the fluid, the motion of the microtubule will follow that of the fluid along the backbone locations. However, due to the long range of the hydrodynamic interaction, the system can now be far more sensitive to the overall configuration, which could potentially lead to more complex steady state solutions than we found for the non interacting single microtubule solutions of Sec. 4.

There are three primary generators of force; backbone stiffness, a gradient in backbone tension, and the kinesin motors. The first two force densities can be computed entirely from the microtubule configuration, and these values can then be used as inputs to the Oseen tensor. The force due to the kinesin coupling and walking is difficult to analyze, however, we will show that it has negligible effect on the long range fluid motion. We will see that this somewhat paradoxical situation still leads to long range fluid flow, as we will discuss below.

5.3 Kinesin Quadrupole

In order for the kinesin to drag the impeller along, it must push against the microtubule, so the force moving the impeller through the fluid has a corresponding opposite force on the microtubule by Newton's third law. Both of these forces are then transmitted to the fluid, so it is reasonable to try to express these forces as some multipole expansion in a small parameter. The microtubules have a significant stiffness which leads to a characteristic buckling length as described in Eq. S-25, which sets a size scale for features of the microtubule motion. Compared to this size scale, the impellers are very small, and bound very tightly to the microtubule backbone. In addition to this,

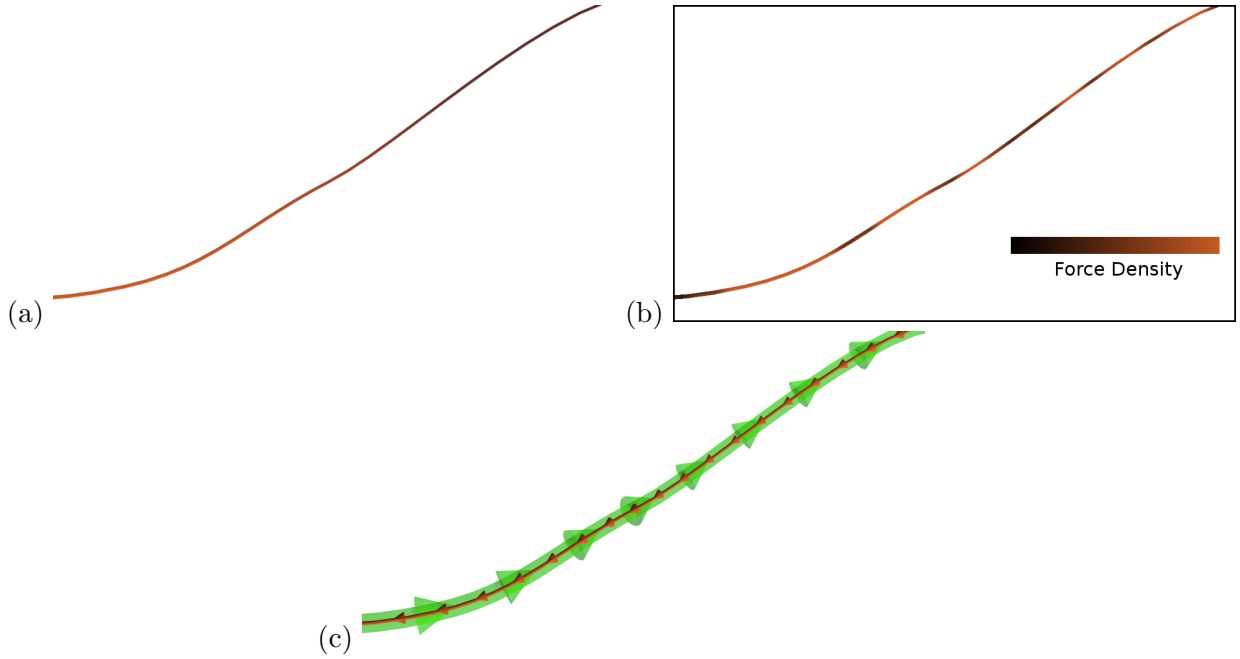

Figure S8: (a) A gradient in tension creates a force density along the axis of the microtubule backbone. This is determined by the microtubule configuration. (b) The microtubule curvature creates a force density (black low and red high) that acts on the fluid. This is also determined by the microtubule configuration. (c) The kinesin motors act on both the microtubule (red arrows) and the impellers (green arrows), applying forces that bind them together and drive the impellers along the microtubule. Both of these force densities are transmitted to the fluid. These force densities arise due to a local coupling, and therefore are related by Newton's third law.

we assume that the impellers are attached to the microtubule in a cylindrically symmetric fashion. This leads to a small scale force distribution that looks like a classic quadrupole configuration, as shown in Fig. S9.

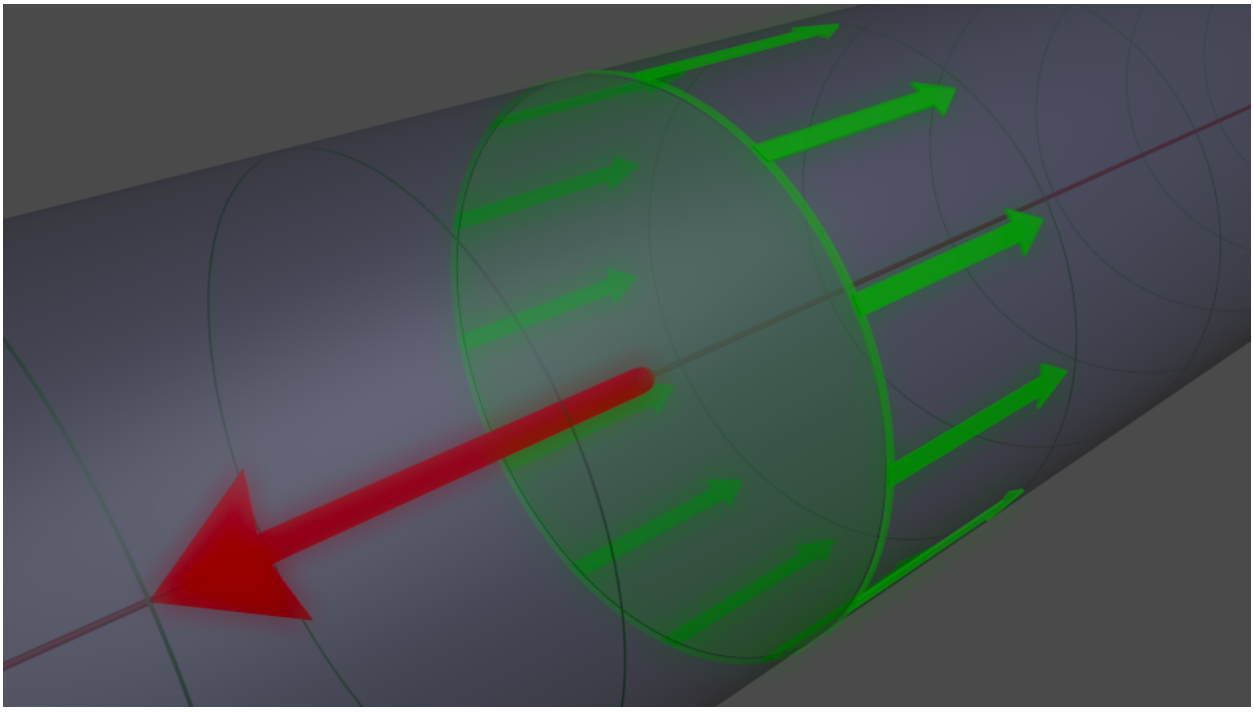

Figure S9: At a given location along the microtubule (maroon line), the forces generated by the kinesin motors push on the microtubule and the impellers in opposite directions. This force density has a cylindrically symmetric shape, which contributes to a rapid falloff in the effect it has on the fluid.

We next investigate the contribution to the fluid velocity field from a small segment of the microtubule impeller system. For convenience, place the segment at the origin, and calculate the fluid motion at position $\mathbf{r}$. The kinesin motors apply force between the microtubule and impellers in two ways. They walk along the axis of the microtubule producing significant force along the

axis, and they also hold the impellers onto the microtubule, creating a rigid link force radially. A key feature of the nature of these forces is symmetry of inversion through the center axis.

We can now write down the fluid response due to this force density.

$$\delta\mathbf{u}(\mathbf{r}) = \frac{1}{8\pi\mu}\int \frac{\mathbf{f}}{|\mathbf{r}+\mathbf{a}|} + \frac{(\mathbf{r}+\mathbf{a})((\mathbf{r}+\mathbf{a})\cdot\mathbf{f})}{|\mathbf{r}+\mathbf{a}|^3}d\hat{\mathbf{a}} - \frac{\mathbf{F}}{|\mathbf{r}|} - \frac{\mathbf{r}(\mathbf{r}\cdot\mathbf{F})}{|\mathbf{r}|^3} \tag{S-31}$$

Where $\delta\mathbf{u}(\mathbf{r})$ is the contribution to the fluid velocity at position $\mathbf{r}$ from a differential segment of the microtubule impeller system, a is the vector pointing from the center of the microtubule to a point in the impeller sheath, F is the linear force density on the microtubule backbone produced by the kinesin walkers, and f is an area force density of the force needed to drag the impeller sheath through the fluid. Because the kinesin binds the microtubule and the impeller together, Newton's Third Law dictates that the linear force density along the backbone needs to be equal and opposite for the impeller microtubule pair. This gives us that integrating f around the full circle must give the same value as F. Due to the small size of the kinesin molecule, for long range interaction on the order of the length of the microtubule, or even characteristic curvatures of the microtubule, we should have $a << r$, where a and r are the magnitudes of $\mathbf{a}$ and $\mathbf{r}$ respectively. We can pull out a factor of r to obtain these expressions in terms of a unit-less small parameter $\epsilon = a/r$.

$$\int \frac{\mathbf{f}}{|\mathbf{r}+\mathbf{a}|} + \frac{\mathbf{r}(\mathbf{r}\cdot\mathbf{f})}{|\mathbf{r}+\mathbf{a}|^3}d\mathbf{a} \tag{S-32}$$

Becomes

$$\int \frac{\mathbf{f}}{r|\hat{\mathbf{r}}+\epsilon\hat{\mathbf{a}}|} + \frac{(\hat{\mathbf{r}}+\epsilon\hat{\mathbf{a}})((\hat{\mathbf{r}}+\epsilon\hat{\mathbf{a}})\cdot\mathbf{f})}{r|(\hat{\mathbf{r}}+\epsilon\hat{\mathbf{a}})|^3}d\hat{\mathbf{a}} \tag{S-33}$$

Apart from a global factor of $1/r$, only the directions of $\mathbf{r}$ and $\mathbf{a}$ remain, with all of the distance scaling being absorbed into the small parameter ϵ. We can now expand the expression to find what the leading order contribution to the fluid velocity field will be. The zeroth order term reduces simply to

$$\delta\mathbf{u_0}(\mathbf{r}) = \int \frac{\mathbf{f}}{r|\hat{\mathbf{r}}|} + \frac{(\hat{\mathbf{r}})(\hat{\mathbf{r}}\cdot\mathbf{f})}{r|(\hat{\mathbf{r}})|^3}d\hat{\mathbf{a}} - \frac{\mathbf{F}}{|\mathbf{r}|} - \frac{\mathbf{r}(\mathbf{r}\cdot\mathbf{F})}{|\mathbf{r}|^3} \tag{S-34}$$

Which will vanish due to the requirement of Newton's Third Law. The first order term in ϵ requires a bit more work, but is still a straightforward derivative. We first need to expand the magnitudes

in terms of a square root as follows,

$$\delta\mathbf{u}(\mathbf{r}) = \frac{1}{r}\int \mathbf{f}[(\hat{\mathbf{r}}+\epsilon\hat{\mathbf{a}})^2]^{-1/2}d\hat{\mathbf{a}} + (\hat{\mathbf{r}}+\epsilon\hat{\mathbf{a}})(\hat{\mathbf{r}}+\epsilon\hat{\mathbf{a}})\cdot\mathbf{f}[(\hat{\mathbf{r}}+\epsilon\hat{\mathbf{a}})^2]^{-3/2}d\mathbf{a} - \frac{\mathbf{F}}{|\mathbf{r}|} - \frac{\mathbf{r}(\mathbf{r}\cdot\mathbf{F})}{|\mathbf{r}|^3} \tag{S-35}$$

$$\begin{aligned}
\tfrac{d}{d\epsilon}\delta\mathbf{u}(\mathbf{r}) &= \tfrac{1}{r}\textstyle\int -\mathbf{f}[(\hat{\mathbf{r}}+\epsilon\hat{\mathbf{a}})^2]^{-3/2}(\hat{\mathbf{r}}+\epsilon\hat{\mathbf{a}})\cdot\hat{\mathbf{a}} \\
&+ \hat{\mathbf{a}}(\hat{\mathbf{r}}+\epsilon\hat{\mathbf{a}})\cdot\mathbf{f}[(\hat{\mathbf{r}}+\epsilon\hat{\mathbf{a}})^2]^{-3/2} \\
&+ (\hat{\mathbf{r}}+\epsilon\hat{\mathbf{a}})(\hat{\mathbf{a}}\cdot\mathbf{f})[(\hat{\mathbf{r}}+\epsilon\hat{\mathbf{a}})^2]^{-3/2} \\
&- 3((\hat{\mathbf{r}}+\epsilon\hat{\mathbf{a}})(\hat{\mathbf{r}}+\epsilon\hat{\mathbf{a}})\cdot\mathbf{f}[(\hat{\mathbf{r}}+\epsilon\hat{\mathbf{a}})^2]^{-5/2}(\hat{\mathbf{r}}+\epsilon\hat{\mathbf{a}})\cdot\hat{\mathbf{a}}
\end{aligned} \tag{S-36}$$

$$\begin{aligned}
\lim_{\epsilon\to 0}\tfrac{d}{d\epsilon}\delta\mathbf{u}(\mathbf{r}) &= \tfrac{1}{r}\textstyle\int -\mathbf{f}[(\hat{\mathbf{r}})^{\mathbf{2}}]^{-\mathbf{3/2}}(\hat{\mathbf{r}})\cdot\hat{\mathbf{a}} \\
&+ \hat{\mathbf{a}}(\hat{\mathbf{r}})\cdot\mathbf{f}[(\hat{\mathbf{r}})^2]^{-3/2} \\
&+ (\hat{\mathbf{r}})(\hat{\mathbf{a}}\cdot\mathbf{f})[(\hat{\mathbf{r}})^2]^{-3/2} \\
&- 3((\hat{\mathbf{r}})(\hat{\mathbf{r}})\cdot\mathbf{f}[(\hat{\mathbf{r}})^2]^{-5/2}(\hat{\mathbf{r}})\cdot\hat{\mathbf{a}}
\end{aligned} \tag{S-37}$$

As we can see, each term in the integrand is an odd function of $\hat{a}$, and the integral is around the whole circle, so this vanishes. This means that the leading order term from the kinesin coupling force density is going to be suppressed by two factors of the small parameter ϵ. In comparison, the tension can be decomposed into equal and opposite pairs between adjacent segments of the microtubule. However, we will find that they are not able to form a quadrupole like the kinesin forces do. The separation between the two opposing forces is axial, and lacks the mirror symmetry needed to form the quadrupole. This means that it would give rise to a dipolar term. And even in the case of the dipolar term, the corresponding small parameter needed to form the multipole cancellation is directly tied to the characteristic length scale of the microtubule curvature; indeed, the curvature is defined by these forces. So not only would it be a chain of dipoles, the density of those dipoles would need to diverge in the limit of small separation between the opposing forces. If we instead sum the forces on each individual segment, we are left with the simple linear force density of the gradient of the tension. This gradient is expected to be nonzero due to the tethering of the microtubule minus-end. A nonzero linear force density along the axis of the microtubule would apply directly through the Oseen tensor with no cancellation, and thus fall off as $\mathbf{r}^{-1}$, where

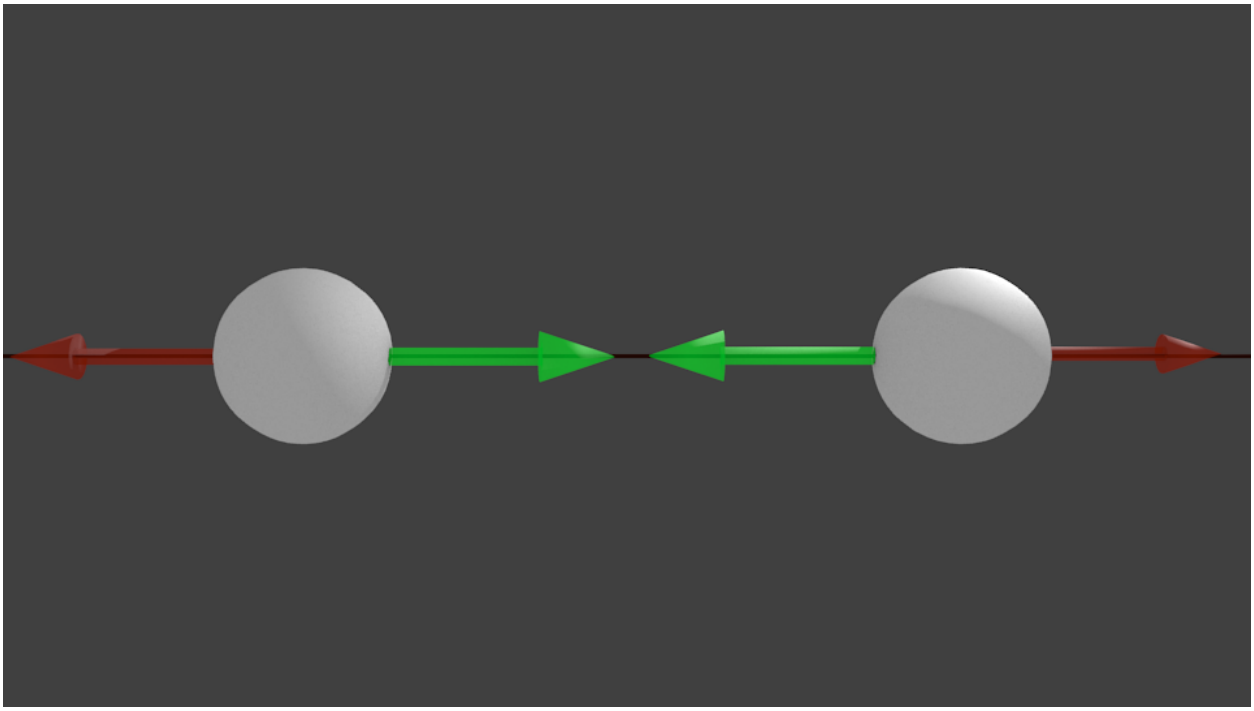

Figure S10: While the forces connecting the microtubule backbone must balance, these forces are a) axial and lack the symmetric cancellation of the quadrupole and b) the separation between them is the basis for the characteristic length scale of the microtubule itself, and is thus fixed in relation to the size scale of the interaction.

as we saw the kinesin forces fall off as $\mathbf{r}^{-3}$. This is not to say that the kinesin does not effect the system at all.

While the long range fluid motion will not be strongly influenced by the kinesin motor forces, these short range effects will allow the impellers and microtubule to move relative to each other. While the details of the local fluid motion are complex, the bulk effect is known; the kinesin walks along the microtubule at a steady rate, creating a fixed relationship between the impeller velocity and the microtubule velocity. Because the relative motion between the microtubule and the impeller layer is known, only the motion of the fluid at the impeller interface is needed to determine the motion of the system. As we have shown, the forces due to the kinesin motors directly do not contribute to the long range fluid motion, and the only remaining forces are those from microtubule backbone. Note that this does not contradict the analysis of Sec. 2 where we analyzed the hydrodynamics of a line of impellers. In both cases, the force on the fluid due to the power expenditure of the motors is the same. In the current analysis, we have separated out the internal force-pairs that were lumped together in the previous analysis. Instead of considering fluid flow to be directly caused by forces from the impeller as we did previously, we have considered all the separate elements, kinesin, impellers, tension, and microtubule curvature, that are all coupled to the fluid as expressed by Eq. S-30. What we showed above is that there is a cancellation of the long range fluid flow from the terms involving kinesin forces. The long range flow that remains is due to the tension and curvature terms. Because of Newton's third law, the long range flow in Sec. 2 is the same for these two descriptions.

This leads us to a method for determining the dynamics of the system. The Oseen tensor should be integrated over the force densities f_{int} along the backbone of the microtubule, ignoring the contribution from the impeller directly.

$$\mathbf{u}(\mathbf{r}) = \int_{backbone} \mathbf{f}_{int}(\mathbf{r}') \cdot \mathbf{J}(\mathbf{r} - \mathbf{r}') d\mathbf{r}' \tag{S-38}$$

This will give us the large scale fluid motion that will determine the large scale motion of the entire system. The coupling from the fluid back to the impeller/microtubule system will depend on the

short range fluid interactions brought about by the kinesin motors; however, we still expect the long range motion of the microtubule/impeller system to match that of the fluid. By symmetry, the difference in velocities will be axial, and the kinesin will still maintain a fixed relationship between the microtubule and impeller. From that we expect the fluid velocity to appear to be a weighted average of the microtubule and impeller velocity.

$$\mathbf{u}(\mathbf{r}) = \mathbf{v}_I(1-\delta) + \mathbf{v}_M\delta \tag{S-39}$$

Where $\mathbf{v}_I$ and $\mathbf{v}_M$ are the impeller and microtubule velocities, respectively. If we use the fact that $\mathbf{v}_I - \mathbf{v}_M = v_k\frac{\partial \mathbf{r}}{\partial s}$, we find an expression for our microtubule velocity

$$\frac{d\mathbf{r}}{dt} = \mathbf{v}_M = \mathbf{u}(\mathbf{r}) - (1-\delta)v_k\frac{\partial \mathbf{r}}{\partial s} \tag{S-40}$$

where v_k is the kinesin velocity. As we can see, the effect of the coupling on the microtubule motion is to act as though the kinesin velocity is suppressed by some fraction, relative to if the entire microtubule were covered with kinesin. This is the same result as was obtained in the single microtubule discussion (Sec. 2). While the exact value of this suppression depends on the detailed hydrodynamic interactions of the microtubule and impellers, the large scale behavior can be obtained by a simple rescaling of the walk speed, giving us the relation:

$$\frac{d\mathbf{r}}{dt} = \mathbf{u}(\mathbf{r}) - \mathbf{v}_k\frac{\partial \mathbf{r}}{\partial s} \tag{S-41}$$

5.4 Hydrodynamics near a hard wall

Up until now, we have only considered microtubules pinned at one end and unhindered by any other structures nearby. However our photobleaching tests (Fig. 7) and prior observations agree that microtubules are attached by their minus ends to the oocyte cortex. The presence of this stationary wall may have a significant effect on the microtubule motion, as it imposes a new boundary condition on the fluid motion; namely that the velocity must vanish at the wall.

This new boundary condition changes the Green's function used to construct the fluid velocity from the forces applied to the system. The determination of this Green's function is dependent on

the specific boundary geometry, and potentially intractable. Because of this, we will first investigate the case of an infinite plane hard wall at $z = 0$, to provide some insight into the behavior of the microtubule impeller system near the cortex.

Fortunately, the Green's function for the infinite wall case has already been solved[S10]. The technique is similar to that of the method of image charges in classical electromagnetism, with the added complication of the sources being vector quantities instead of scalers. This vector nature of the sources gives rise to a number of corrections to the simple reflection. It is somewhat complex, though not of higher order scaling than the unmodified Oseen tensor. The interaction $\mathbf{J}^w(\mathbf{x}, \mathbf{y})$ between a point force $\mathbf{f}$ at location $\mathbf{x}$ and a fluid location $\mathbf{y}$ is now:

$$\mathbf{J}^w(\mathbf{x}, \mathbf{y}) \cdot \mathbf{f} = \frac{1}{8\pi\mu\mathbf{r}^*}[-(\mathbf{I} + \frac{(\mathbf{r}^* \cdot \mathbf{f})\mathbf{r}^*}{\mathbf{r}^{*2}}) + \frac{2H}{\mathbf{r}^{*2}}((\frac{3x_3(\mathbf{r}^* \cdot \tilde{\mathbf{f}})}{\mathbf{r}^{*2}}\mathbf{r}^* - \tilde{\mathbf{f}}_3)\mathbf{r}^* - x_3\tilde{\mathbf{f}} + (\mathbf{r}^* \cdot \tilde{\mathbf{f}})\hat{\mathbf{z}})] \qquad \text{(S-42)}$$

Where $\mathbf{r}^*$ is equal to $(x_1 - y_1, x_2 - y_2, x_3 + y_3)$, the reflected displacement vector, $H = y_3$, the distance of the fluid from the wall, and $\tilde{\mathbf{f}} = (f_1, f_2, -f_3)$, the reflected force. One can recognize the first term as the reflected Oseen tensor, similar to a negative charge in the method of images. However, as previously mentioned, the fact that the force must also have its direction flipped adds several additional terms. These terms together ensure that the velocity of the fluid will vanish at the boundary.

Other than the modification of the interaction tensor, the model remains almost unchanged. Due to the assumptions used to generate this solution, it is of course only valid for $z > 0$, and can result in strange behaviors if applied for regions below the plane $z < 0$. These usually result in extremely singular velocities, and so care must be taken to ensure that no part of the finite time step used in a simulation will cross this boundary. To ensure this, a hard wall potential similar to that used for the hard core repulsion of the microtubule segments is placed at $z = 0$, as will be described in more detail below in Sec. 5.6.

5.5 Numeric Implementation of the Model

The complexity of the interaction makes analytic solutions difficult, however, the dependence of the fluid flow only on the current state of the microtubule makes it suitable for direct simulation. A straightforward integration of the velocity field will yield the complete system dynamics.

5.6 The discrete model

As with the single microtubule case, the microtubules are modeled as a chain of discrete points. The use of the long range fluid interactions prevents us from using pure rigid links, so this model uses a backbone comprised of stiff spring links, such that the force on each element is:

$$\mathbf{T}(\mathbf{r}_i) = k_T(|\mathbf{d}_{i-}| - l)\hat{\mathbf{d}_{i-}} + (|\mathbf{d}_{i+}| - l)\hat{\mathbf{d}_{i+}} \tag{S-43}$$

With

$$\begin{aligned} \mathbf{d}_{i-} &= \mathbf{r}_{i-1} - \mathbf{r}_i \\ \mathbf{d}_{i+} &= \mathbf{r}_{i+1} - \mathbf{r}_i \end{aligned}$$

Where $\mathbf{r}_i$ are the positions of the individual microtubule segments, with k_T being the backbone spring constant and l being the rest length of the segment. The spring constant is chosen to be as strong as possible for the given time step, in order to match as closely as possible to an incompressible chain. In addition to the spring force tension term, the backbone stiffness is modeled as a discrete fourth derivative along the spine, with an adjustable scaling parameter.

$$\mathbf{C}(\mathbf{r}_i) = -k_C[(\mathbf{r}_{i+2} - \mathbf{r}_i) - (\mathbf{r}_i - \mathbf{r}_{i-2})] \tag{S-44}$$

In order for the microtubules to not cross through each other, they are also given a hardcore repulsion force that is divergent at zero distance along with rapidly and smoothly falling off to zero at some characteristic radius d. This was implemented as a inverse fourth power law with a cutoff. In addition we also allowed for an attractive interaction between microtubules over a shell spanning

$d < r < d_a$, which we added as an explanation of the bundling of microtubules that is apparent in movies of fast streaming:

$$\mathbf{f_h}(\mathbf{\Delta r}) = \begin{cases} (1 - \frac{d^4}{\Delta r^4})\mathbf{\Delta r}, & \text{for } \Delta r < d \\ -\frac{32 * f_a}{(d_a - d)^2}(\Delta r - d)(\Delta r - d_a)(2\Delta r - d - d_a)\frac{\mathbf{\Delta r}}{\Delta r}, & \text{for } d < \Delta r < d_a \\ 0, & \text{for } \Delta r \geq d_a \end{cases} \tag{S-45}$$

$$\mathbf{f_H}(\mathbf{r}_i) = \sum_j \mathbf{f_h}(\mathbf{r}_i - \mathbf{r}_j) \tag{S-46}$$

The attractive force is normalized so that the minimum depth of the corresponding potential is $-f_a$.

In addition to the bulk forces, there are also boundary cases, as well as tethering the minus-ends of the microtubule. The tethering is accomplished simply by including a spring force, similar to the tension spring force, that is centered to a specific fixed point in space. All of these forces are directly transmitted to the fluid, and thus must be included in the Oseen tensor calculation. There is a difficulty when transitioning to the discrete case due to the singularity of the Oseen tensor at the origin. For this reason, the effect of the forces generated on a specific segment on the fluid at the same location is more difficult to determine. The standard practice in this case is to use the Oseen tensor as an interaction between elements, and to use a simple free draining drag model for the local motion. Since our microtubule is modeled as a long chain of beads we simply use the drag due to a small sphere

$$\mathbf{J}_{ii} = \frac{1}{4\pi\mu}. \tag{S-47}$$

By combining equations S-43, S-45, S-44, and S-38, we see that for any point in space, the fluid velocity is given by:

$$\mathbf{u}(\mathbf{r}_i) = \mathbf{J}_{ii}[T(\mathbf{r}_i) + C(\mathbf{r}_i) + H(\mathbf{r}_i)] + \sum_{j \neq i} \mathbf{J}(r_i - r_j)[\mathbf{T}(\mathbf{r}_j) + \mathbf{C}(\mathbf{r}_j) + \mathbf{f_H}(\mathbf{r}_j)] \tag{S-48}$$

However, due to the relative velocity between the fluid and the microtubule backbone, the velocity used to update the position of the microtubule locations r_i is found by subtracting the kinesin walk speed.

$$\frac{d\mathbf{r}_i}{dt} = \mathbf{u}(\mathbf{r_i}) - \frac{\mathbf{1}}{\mathbf{2}}\mathbf{v_k}(\mathbf{r_{i-1}} - \mathbf{r_{i+1}}) \tag{S-49}$$

This derivative is then used for a standard fourth order Runge Kutte integration in order to advance the system in time.

5.7 Single Microtubule verification

The new algorithm was then used to simulate a single microtubule in order to see what effect the fluid interaction would have on the single microtubule solution. Because this simulation does not apply any external flow fields, we expect the solution to closely resemble the zero field case from the theory without fluid coupling (see Sec. 4).

We ran this simulation using the same parameters for a single microtubule with and without the fluid interaction, again using a random starting configuration and tethering the minus-end of the microtubule to a fixed point in space. The result was essentially as expected, with a solution that asymptotically approached a circle rotating at a constant rate (Fig. S11).

It is interesting to note that the hydrodynamic interaction has little to no effect on this type of solution.

5.8 Properties of the Many Polymer Model

More microtubules are added to the simulation, so that there are on the order of tens to hundreds of them. The microtubules have their minus ends tethered in a planar configuration, to mimic tethering to the cortex. Spacing between the individual anchors can be varied, but will never be close enough for their hardcore radii to overlap.

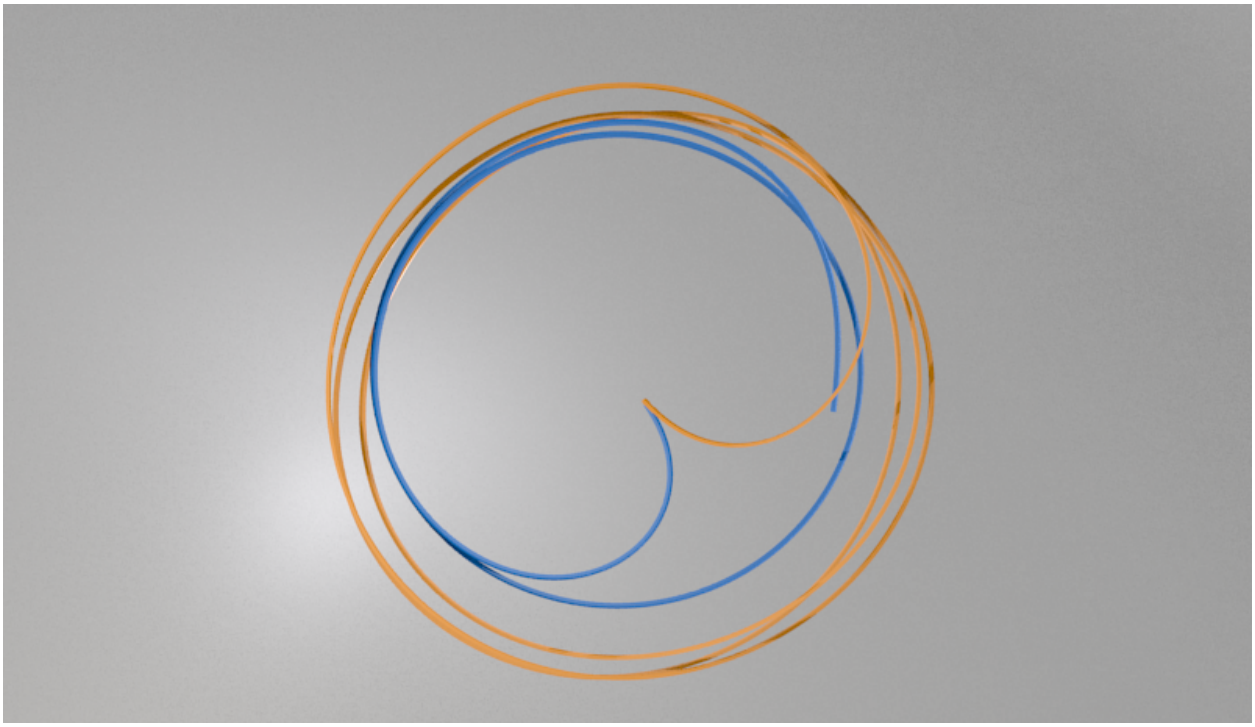

Figure S11: Simulation results for a single polymer without fluid interaction(blue) and with fluid interaction(orange), with all other parameters held the same. Both polymers are tethered at the center of the image, near the center of the circular configuration. The images are super imposed, but the polymers were simulated separately. They are qualitatively the same, though the radius is slightly larger with fluid interactions activated.

5.9 Important Length Scales

The introduction of more than one microtubule, along with the addition of the hard wall, introduces new length scales to the system. The microtubules are placed with their tether points in a plane parallel to the hard wall, each initialized with a random configuration subject to the constraint that they not pass through the wall. Within this plane, the tethered minus ends have a characteristic separation, R_s, and this separation defines one of the new length scales in the system.

In the oocyte, the hard wall is the plasma membrane and a closely associated dense meshwork of proteins, including filamentaous actin. Inward from that, the f-actin meshwork becomes less dense. The inward side of this cortical meshwork is loose enough to allow fluid flow, but able to tether microtubules such that their initial point of bending (tether point) is at some distance away from the impenetrable oocyte wall. For this reason we study microtubule patches that are at some small fixed distance H away from the hard wall boundary. Although the real situation involves a more complicated flow, due to the meshwork described above, we expect that this should be similar to our system with H chosen appropriately. In addition, the means by which they are attached may hinder rotation about the attachment, so if they are pointing perpendicular to the oocyte wall, then they will be effectively raised from it. For these reasons, we take the separation between the plane of the hard wall and the plane of anchors, H, to be nonzero. This represents a second new length scale.

These two new lengths are set to be less than the characteristic buckling length of the microtubule, R_b, in order to more closely match what is seen in the biological data. We will see that these two length scales play an important role in determining the correlation behavior of the system.

5.10 Correlation Between Multiple Microtubules

A key feature found during fast streaming is the formation of correlated groups to enable larger scale coordinated forces on the fluid. These correlations arise as the motion of fluid near a microtubule causes that microtubule to align with the preexisting flow. The microtubules contribute to that

flow because a type of field amplification occurs. Essentially, the long range interaction through the cytoplasmic fluid could bring about a transition to a phase of long range order.

When the simulation is run with a small number of microtubules placed with their tethered minus-ends near each other (less than the microtubule buckling length), short range correlation almost always emerges. Using a random walk starting condition, the microtubules initially fall into seemingly independent circular solutions similar to those of the single microtubule case. However, after a few periods of revolution the microtubules eventually collapse into one circular solution (see Fig. S12).

While this correlation is a promising feature, it is not enough to produce a long range directed flow field, particularly because of the circular nature of the motion. To sustain linear streaming, the forces transmitted to any one microtubule from the rest of the system need to be stronger than the local kickback force from the kinesin motors. A small number of microtubules will not be able to achieve this.

5.11 Microtubule Patches

To attain linear streaming in our simulation, we include more microtubules. These microtubules are placed with their minus-end anchor points in a square grid, and then some small random jitter is applied within the plane to their positions. The random noise is added to suppress periodic lattice effects, which should not be present in the cell. Once the anchor points are chosen, the microtubules are initialized with a random walk biased slightly in the positive z direction to avoid problems caused by starting in the hard wall. Any configuration that penetrates the wall is rejected. Due to the random nature of the initial conditions, the microtubules often start with high curvatures. This causes the first few steps of the simulation to be dominated by the microtubules rapidly relaxing to their more typical curvature. This artifact of the somewhat artificial initial conditions should not be relevant to the actual biological system, so these initial steps are not shown. The forces that cause this relaxation are quite high, and occasionally they can cause the microtubules

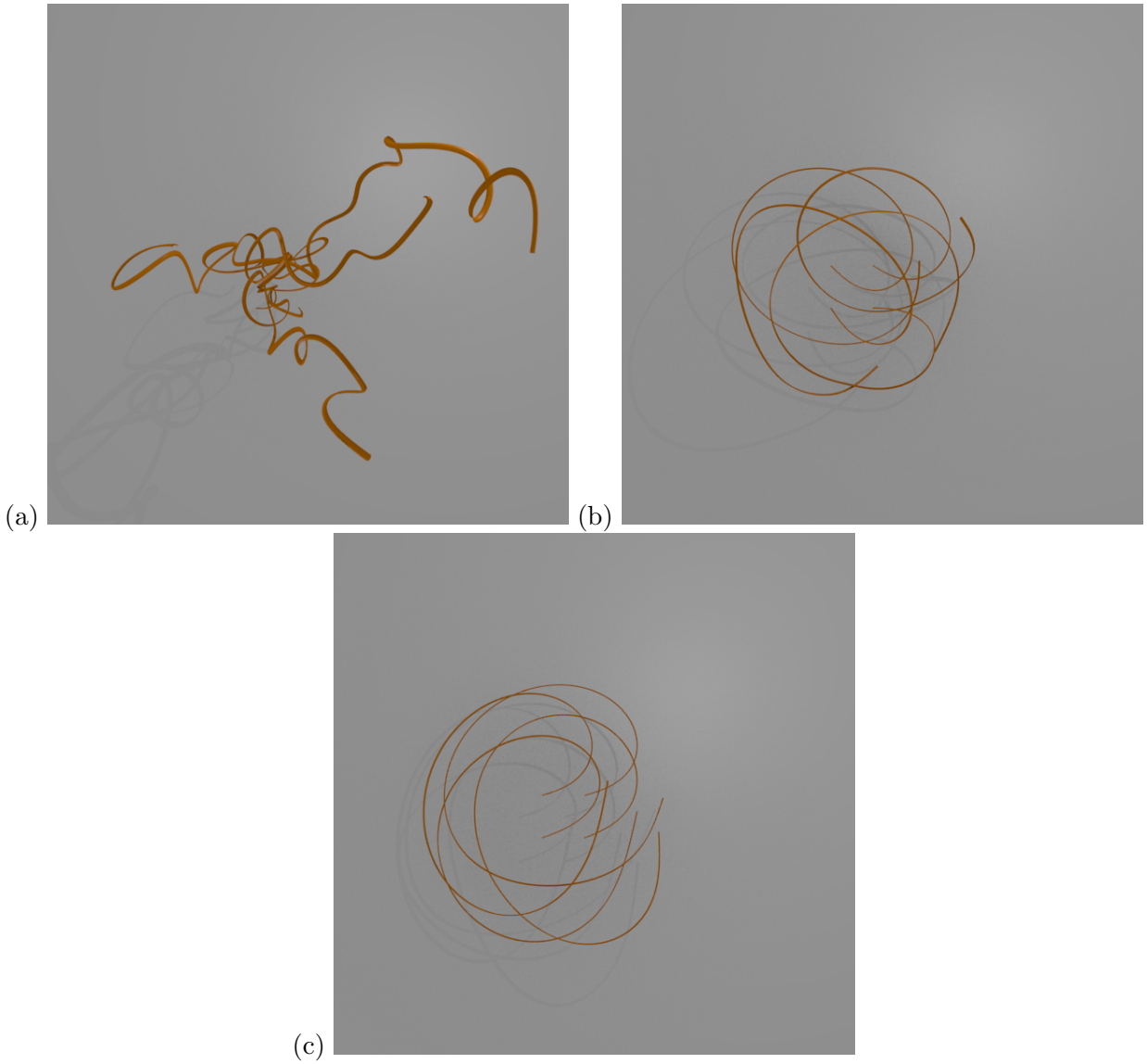

Figure S12: (a) A typical starting configuration of four microtubules, with $R_s = 2$ and $H = 2$. The apparent thickness is an artifact of the display method. (b) After a short time, the microtubules fall into individual circular solutions, with some correlation. (c) After a few revolutions, all of the microtubules collapse into correlated circles.

to break through the hard wall. This most often results in a divergence due to the hard wall Oseen tensor having odd behavior for negative z values. Initial conditions that lead to this effect are also rejected. A typical initialized patch is shown in Fig. S13 To check that these extreme initial conditions were not influencing our final steady state behavior, and to improve the realism of the model, we employed a Monte Carlo algorithm to initially anneal the chains to give more realistic curvatures. This greatly improved the robustness of our initial configurations preventing the breakthroughs mentioned above. However, it had no discernable effect on the steady state behavior despite testing the simulation with a wide variety of different conformations.

5.12 Linear Streaming with Microtubule Patches

There is a fairly wide range of parameters for which, regardless of the random initialization, the microtubule patch will self organize into a stable directed flow (Fig. S14).

The length of time needed for the patch to reach this linear streaming phase can vary based on the parameters of the simulation, but in general it will be within a few periods of the single microtubule rotation. During this correlation time, smaller sub regions of extended microtubules appear. These sub regions can slowly rotate as a unit, and tend to cause more microtubules to correlate along with them as they pass nearby. Once established, the linear streaming regions are stable and settle into a single direction.

It is important to re-emphasize that there is no externally imposed fluid motion in this simulation, and that the linear configuration is brought about by fluid mediated interactions between microtubules. The final direction of the array and of streaming is dependent on the exact nature of the random initial conditions, which are not guaranteed to be perfectly isotropic. The spontaneous generation of this ordered phase will cause some aspects of the resulting system, such as the direction of the resulting global flow field, to depend sensitively on the initial conditions of the system. However, many properties of the system in this phase, such as the flow speed and characteristic oscillation frequencies, should be independent of the initial conditions. As long as the microtubules

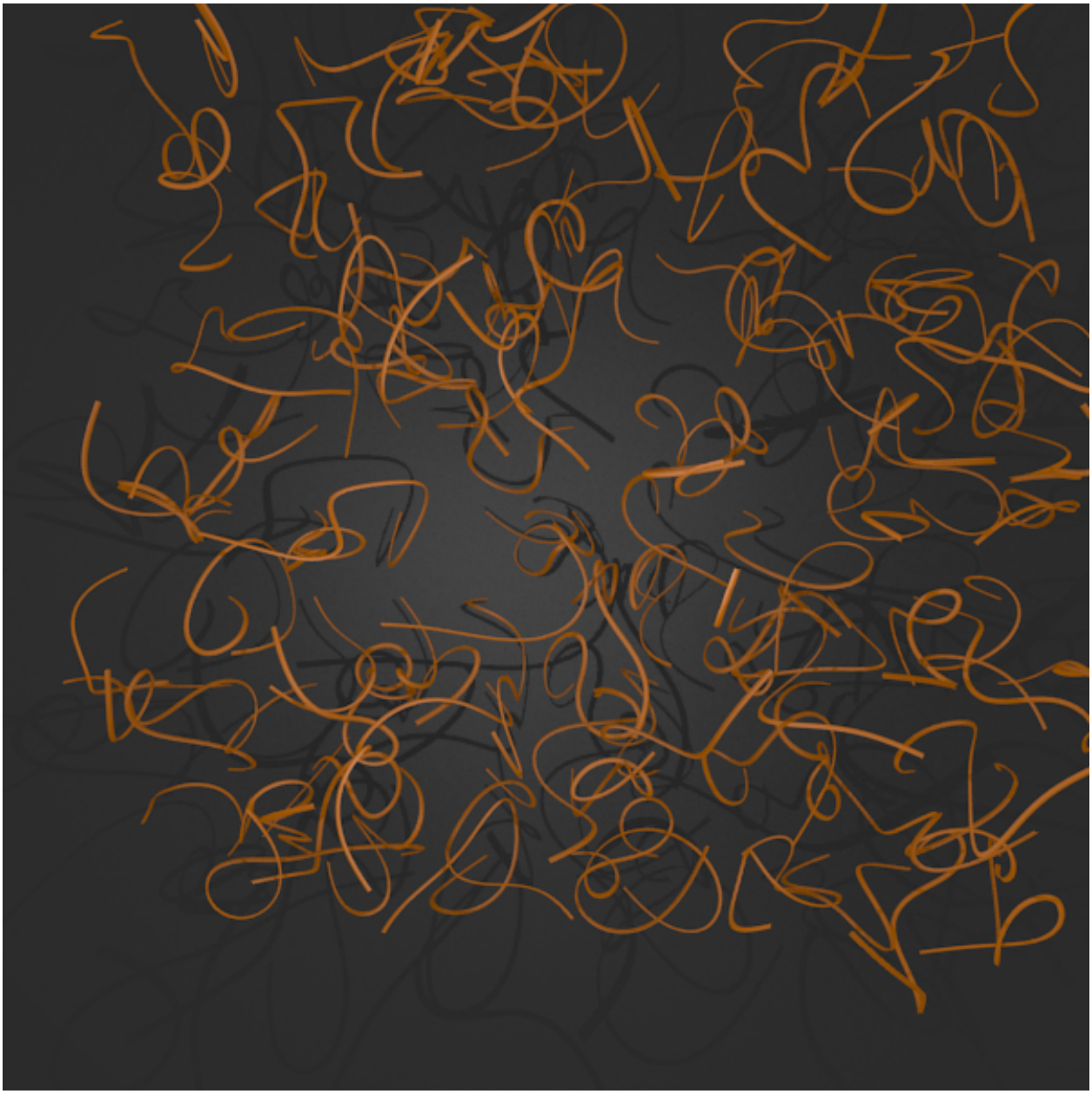

Figure S13: A typical starting configuration for a microtubule patch, viewed from directly above the plane of the hard wall. The microtubules are tethered at their minus ends in a square grid pattern above the wall by the same distance as the separation between the anchor points. The grid of anchor points occupies the majority of the view, though it is slightly shifted to give a better view of the microtubules.

Figure S14: A typical configuration after correlation, viewed from an angle to better show the planar nature of the solution. The grid of anchor points is significantly farther from the hard wall boundary in this simulation than was used in the previous image, in order to increase long-range correlation. The microtubules minus-ends are tethered at their rightmost endpoint in this image, and the fluid flow is left and upward, away from the viewer. The microtubules on the edges of the patch can be seen to execute a helical pattern reminiscent of the single microtubule dynamics.

are essentially at rest in a steady state, the fluid velocity should be determined by the analysis in Sec. 2.

5.13 Disordered Solutions

For some ranges of input parameters, the system does not align well enough to create the fast linear streaming phase. When the fluid interaction forces are not sufficient to overcome the kinesin reaction force, individual microtubules buckle and begin rotating around their tether points. Even though the hydrodynamic interaction is not strong enough to force a straight line solution, it can still cause the rotational solutions to correlate with each other, much like in the case of just a few microtubules (see Sec. 5.10 above). Regions of correlated microtubules can develop (Fig. S15). The dynamic correlations found in this phase might include large numbers of microtubules, but rarely include the anchor points. These masses of loose microtubule ends tend to flow back along their length, and as such generate very little long range fluid motion.

5.14 Conditions for Linear Streaming

Not all microtubule patches will reach the linear streaming phase from a random initial condition. There are ranges of parameters for which the system will only exhibit short range correlation, often in the same manner as the systems with only a few microtubules. In these cases the forces from the fluid interaction are not strong enough to overcome the local kinesin reaction force, and the microtubules buckle and rotate around their anchor points.

Whether a system will reach the correlated directed fast streaming phase is determined by a number of parameters that effect the relative strength of the forces in the system. These parameters can be the internal properties of the microtubule/impeller system, or properties of the arrangement of the microtubules in the patch.

In the next section we will investigate the effects of a wall on the system's propensity for linear streaming and show that it plays an important role.

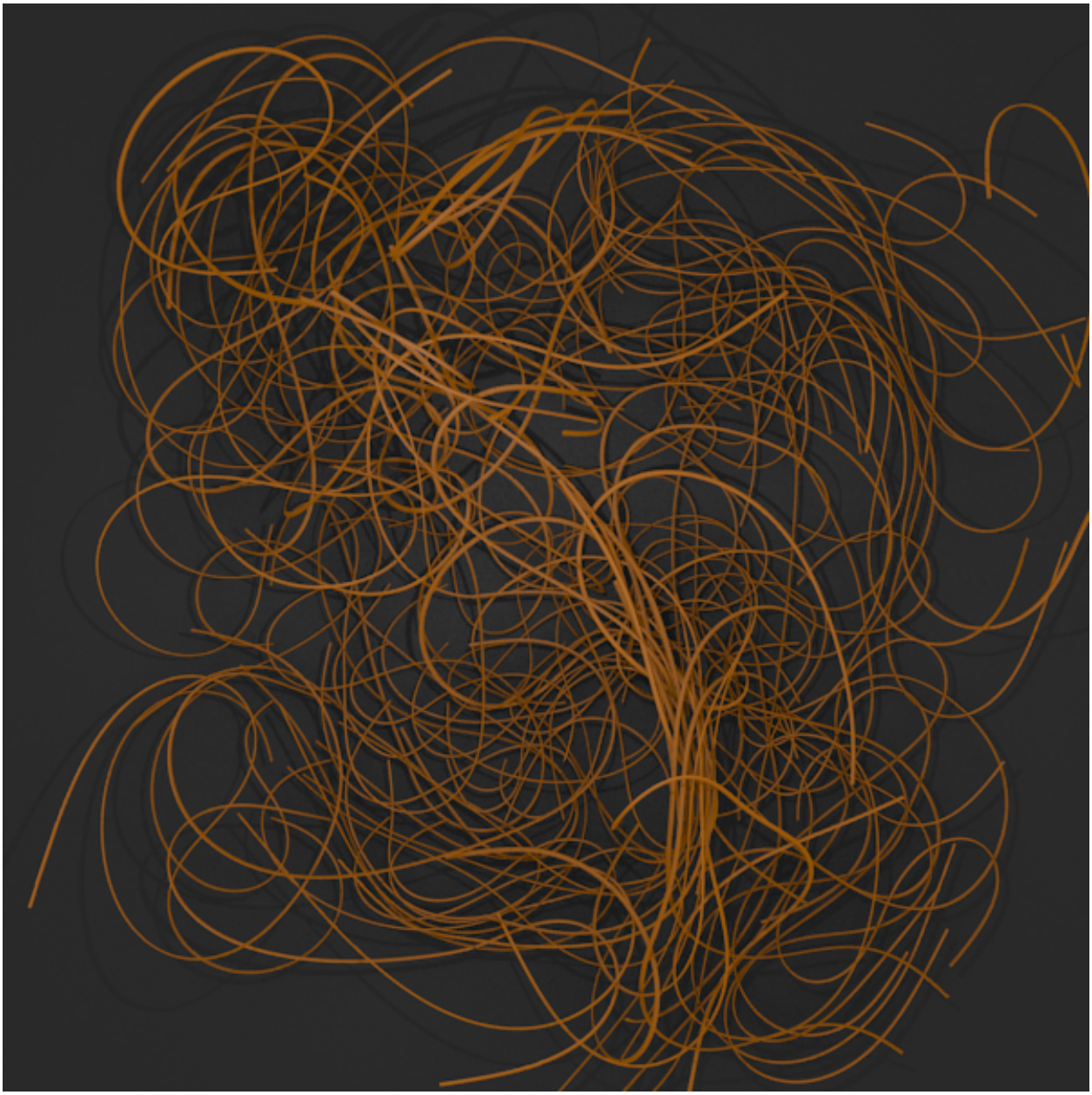

Figure S15: A system that does not achieve directed fast streaming. It does show temporary local correlations, but these are not stable in any one direction.

5.15 Effects of the wall

The hard wall serves to damp out fluid motion near its surface due to its strong interaction with the fluid viscosity. This is seen in the interaction tensor as a negative force mirrored across the wall, opposing the motion of the true force above it. One can imagine that, much like the case in electromagnetism, these mirror forces could form some sort of dipolar arrangement. This arrangement would have faster falloff with distance and could easily interfere with the ability of the entire system of microtubules to correlate over large distances. We can see this effect in the simulation by simply placing the microtubule patch at several distances from the wall while holding the other parameters fixed (Fig. S16).

At large elevations above the wall, the patches reach the linear streaming phase from the random initial state quite rapidly(within only a few rotation periods). As the elevation is decreased, the time the system takes to reach the linear streaming state increases.

Eventually, the wall decreases the interaction strength significantly enough that the nucleation of the linear streaming regions cannot occur. At these distances, the microtubules will often still correlate, but do not manage to achieve the straight line configuration.

5.16 Relative Viscosity

One can also vary the viscosity of the fluid in this system. As can be seen from Eq. S-48 and S-29, there is a global factor of μ^{-1} on all of the driving force terms. Changing the viscosity on any given system will then inversely effect the fluid velocity field from any given set of forces. At first, it might seem that this would only cause a change in the overall timescale of the dynamics, but that turns out to be incorrect. The motion of the microtubule itself is given by Eq. S-49, which includes a term only proportional to the kinesin walk speed. If this speed remains unchanged, the effect of the kinesin forces will be scaled proportionately to the viscosity.

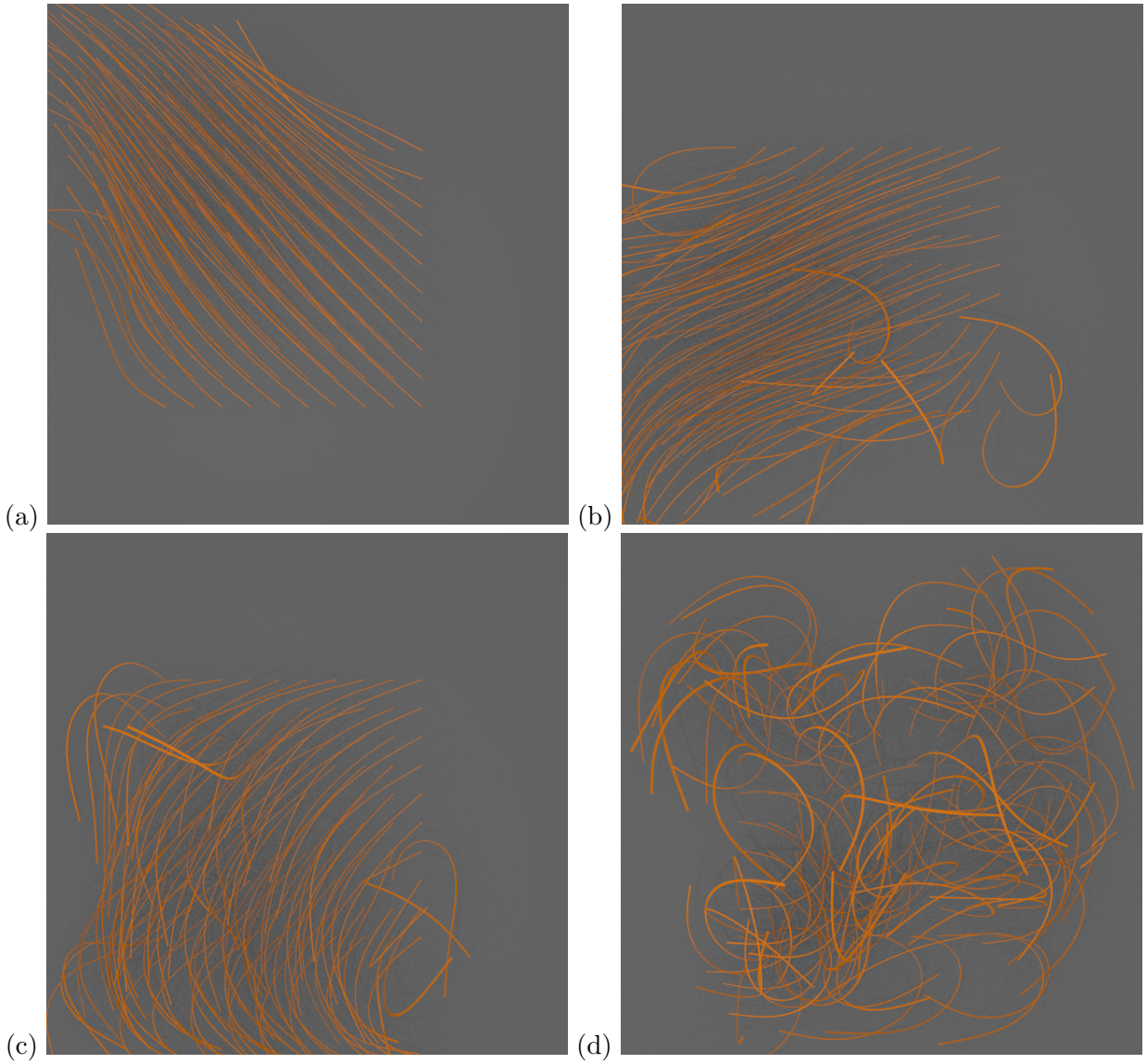

Figure S16: (a-d) Configuration of microtubule patches after 200 simulation frames. (a)Patch at $H = 5$, shows strong directed streaming (b)Patch at $H = 3$, shows directed streaming, but with more loose edges (c)Patch at $H = 2$, shows directed streaming, but propagates large correlated "waves" and is not as straight (d)Patch at $H = 1$, shows no directed streaming, only short range correlated circular motion.

5.17 Hysteresis of Streaming

Because it is a self reinforcing effect, the fast streaming behavior could very easily depend on the initial configuration of the microtubules. For instance, it is believable that a system could be just barely able to support streaming with the microtubules aligned, but that such a system would be unable to spontaneously generate that alignment. This divides our phase space up into additional regions. One region is where the system always transitions to correlated streaming. One would imagine that this region would be one where interactions between microtubules are strong and long range compared to the other length scales in the system. Another region is one where the system can support fast, correlated streaming, but may only reach it from certain classes of initial configurations. This region is obviously less robust if the intent is to achieve fast streaming. A third region is one in which the system can never support fast correlated streaming. This would most likely be a region in which the interaction between microtubules is cut off at a range less than the typical spacing between microtubules.

We focus here primarily on the transition from disordered microtubules into correlated fast streaming. This focus comes from the behavior of the cell during the stages before and after the start of fast streaming. In the oocyte, microtubules are observed to be largely non-correlated or correlated in circular motions during the slow streaming phase (Movie S1), while they are observed in strongly correlated arrays during fast streaming (Movies S2 and S3). The oocyte likely undergoes changes in key streaming parameters to cross the phase boundary from weakly correlated slow steaming to strongly correlated fast streaming. It is well known that reductions in cytoplasmic f-actin and an inward shift of microtubule minus ends coincide with the shift from slow to fast streaming [8,15,16,36].

Supporting References

[S1] Meyhöfer, E. and Howard, J. (1995). "The force generated by a single kinesin molecule against an elastic load." Proc. Natl. Acad Sci. USA. **92** 574-578.

[S2] Yin, H. L. and Stossel, T. P. (1979). "Control of cytoplasmic actin gelsol transformation by gelsolin, a calcium-dependent regulatory protein." Nature **281**, 583-586.

[S3] Cushman, R. H. and Bates, L. M. (1997). "Global aspects of classical integrable systems." Birkhäuser (Basel, Boston, Berlin), Ch. IV.

[S4] Kessler, D. A., Koplik, J., and Levine H. (1985). "Geometrical models of interface evolution. III. Theory of dendritic growth." Phys. Rev. A **31** 1712-1717.

[S5] Barbieri, A., Hong, D. C., Langer, J. S. (1987). "Velocity selection in the symmetrical model of dendritic crystal growth." Phys. Rev. A **35** 1802-1808.

[S6] Deutsch, J. M. (1988). "Theoretical Studies of DNA During Gel electrophoresis." Science **240** 922-924.

[S7] Deutsch, J. M. and Madden, T. M. (1989)."Theoretical Studies of DNA During Gel electrophoresis." J Chem. Phys. **90** 2476-2485.

[S8] Deutsch, J. M. (2010). "Internal dissipation of a polymer." Phys. Rev. E **81**, 061804/(1–6).

[S9] Landau, L. D. and Lifshitz, E. M. (1970). Theory of Elasticity, 2nd ed., Pergamon Press.

[S10] Dabros, T. and van de Ven, T. G. M. (1992). "Hydrodynamic Interactions Between Two Spheres Near a Solid Plane." Int. J. Multiphase Flow **18**, 751-764.